Published by Institute of Physics Publishing for SISSA

Received: *September 21, 2006*
Revised: *January 25, 2007*
Accepted: *February 8, 2007*
Published: *March 6, 2007*

Brane decay of a $(4+n)$-dimensional rotating black hole. III: spin-$1/2$ particles

Marc Casals and Sam Dolan

School of Mathematical Sciences, University College Dublin, Belfield, Dublin 4, Ireland
E-mail: Marc.Casals@ucd.ie, Sam.Dolan@ucd.ie

Panagiota Kanti

Department of Mathematical Sciences, University of Durham, Science Site, South Road, Durham DH1 3LE, United Kingdom
E-mail: Panagiota.Kanti@durham.ac.uk

Elizabeth Winstanley

Department of Applied Mathematics, The University of Sheffield, Hicks Building, Hounsfield Road, Sheffield S3 7RH, United Kingdom
E-mail: E.Winstanley@sheffield.ac.uk

Abstract: In this work, we have continued the study of the Hawking radiation on the brane from a higher-dimensional rotating black hole by investigating the emission of fermionic modes. A comprehensive analysis is performed that leads to the particle, power and angular momentum emission rates, and sheds light on their dependence on fundamental parameters of the theory, such as the spacetime dimension and angular momentum of the black hole. In addition, the angular distribution of the emitted modes, in terms of the number of particles and energy, is thoroughly studied. Our results are valid for arbitrary values of the energy of the emitted particles, dimension of spacetime and angular momentum of the black hole, and complement previous results on the emission of brane-localised scalars and gauge bosons.

Keywords: Large Extra Dimensions, Beyond Standard Model, Black Holes.

JHEP03(2007)019

Contents

JHEP03(2007)019

1. Introduction

The formulation, a few years ago, of theories [1, 2] postulating the existence of additional spacelike dimensions in nature have radically changed the landscape in gravitational physics (for some early works towards this direction, see [3]). Driven by the motivation to address the hierarchy problem, these theories leave unchanged the usual 4-dimensional particle physics by localising the Standard Model (SM) particles on a 4-dimensional brane while allowing the gravitons to propagate in the bulk — the whole of the $(4 + n)$-dimensional spacetime. In the case of the scenario of Large Extra Dimensions [1], in which the additional spacelike dimensions are compact with size L, the latter feature introduces a new fundamental higher-dimensional scale for gravity M_*, that can be significantly lower than the 4-dimensional scale M_P, thus increasing the fundamental Newton's constant — and the strength of gravitational interactions — by orders of magnitude.

An immediate consequence of the above assumption is that particles with energies larger than M_* can probe physics beyond the scale of quantum gravity while their collisions may trigger the appearance of strong gravitational phenomena and lead to the creation of extended objects (p-branes, string balls, string states, etc), rather than ordinary particles, including tiny black holes [4]. This type of trans-planckian particle collision could be

achieved in various environments, such as at ground-based colliders [5] or in high energy cosmic-ray interactions in the atmosphere of the Earth [6] (for an extensive discussion of the phenomenological implications and additional references, see the reviews [7 – 9]). The black holes produced with horizon radius $r_h \ll L$ are submerged into the higher-dimensional spacetime, which modifies their properties (horizon radius, temperature, entropy, life-time etc.) [10]. Nevertheless, they are still expected to go through the same stages in their life as their 4-dimensional counterparts: a short *balding* phase, during which the black hole will shed all additional quantum numbers apart from its mass, angular momentum and charge, the more familiar *spin-down* phase, during which the black hole will lose mainly its angular momentum, then the *Schwarzschild* phase, when the black hole gradually loses its actual mass, and finally the *Planck* phase, where the black hole has reduced to a quantum object with unknown properties.

During the two intermediate phases, the spin-down and Schwarzschild, the black hole loses energy through the emission of Hawking radiation [11] (and through superradiance during the former phase). This will take place via the emission of elementary particles both in the bulk and on the brane, and it will be characterised by a very distinct thermal spectrum. It is this emission spectrum that upon successful detection will provide the most convincing evidence not only for the creation of microscopic black holes but of the very existence of extra spacelike dimensions. For this reason, the emission spectra from a higher-dimensional black hole have been under intensive study over the last few years. Having the simplest gravitational line-element, the Schwarzschild phase was the first one to undergo a systematic study both analytically [12 – 14] and numerically [15]. Both bulk (scalars) and brane (scalars, fermions and gauge bosons) channels were studied, and the derived emission spectra were shown to depend strongly on the number of additional spacelike dimensions in nature, both in terms of the amount of energy and number of particles produced per unit time and of the type of particles produced. More general spherically-symmetric backgrounds were also studied, such as Schwarzschild-de Sitter [16], Schwarzschild-Gauss-Bonnet [17] and Reissner-Nordstrom [18] backgrounds, as well as the effect of the mass of the emitted particles on the spectrum [19]. Recently, the graviton emission rates by a higher-dimensional Schwarzschild black hole were also investigated by a number of authors [20].

After the spherically-symmetric Schwarzschild phase was almost exhaustively studied, the investigation of the form of the radiation spectra for a higher-dimensional rotating black hole was initiated. Two early analytical studies [21, 22] were supplemented, during the last year or so, by a number of works attempting to shed light on this more technically involved case. Exact numerical results for the emission of Hawking radiation from a $(4+n)$-dimensional rotating black hole, in the form of scalar fields on the brane, were first presented in [23]. In that work, the exact value of the angular eigenvalue, that couples the angular and radial part of the equation of motion of the scalar field and does not exist in closed form, was found numerically, and the radial equation was also solved by employing numerical analysis. A comprehensive study of the fluxes of particles, energy and angular momentum for the emission of scalar fields on the brane soon followed [24], that once again presented exact results for the emission rates including the angular distribution of particles. A similar

JHEP03(2007)019

extensive analysis, focussed on the emission of gauge bosons on the brane by a rotating black hole, appeared in [25]. In both of the latter works, it was shown that all emission rates for scalars and gauge fields are greatly enhanced by both the dimension of spacetime and the angular momentum of the black hole. Results produced independently in [26, 27], for these two species of particles, reveal a good agreement between the two sets of analyses. Additional studies in the literature featured the study of the superradiance effect for a higher-dimensional black hole [28] and of the emission in the bulk [29].

Recently, and while this work was in progress, a study [27] produced power and angular momentum emission spectra from a rotating black hole for the last species of brane-localised particles, i.e. fermions. The radial part of the spinor equation was solved numerically with the angular eigenvalue given by an analytical expansion (with terms kept up to 6th order). The power and angular momentum emission spectra were found to exhibit the same characteristics as the ones for scalars and gauge bosons. The present work aims to complete the above analysis by presenting all emission spectra (particle, energy and angular momentum) as well as total emissivities (emission rates integrated over the frequency) and angular distribution of the emitted radiation. To this end, both the radial and angular part of the fermionic equation of motion will be solved numerically, and an exact numerical value for the angular eigenvalue will also be determined and employed in the calculation.

The outline of our paper is as follows: we start, in section 2, with the presentation of the theoretical framework for our analysis, and the derivation of the radial and angular part of the spin-1/2 equation of motion on the brane. The expressions for the transmission coefficients and the various Hawking radiation emission rates, adopted for emission on the brane, are reviewed in section 3. In section 4, the numerical techniques used to integrate the angular and radial parts of the spin-1/2 equation of motion and determine the angular eigenvalue are described. Section 5 presents our numerical results for the transmission coefficient, the particle, energy and angular momentum fluxes, as well as the total emissivities, and their dependence on both the dimension of spacetime and angular momentum of the black hole is investigated. The angular distribution of the particle and energy emission rates are also studied by using the exact values of the spin-1/2-weighted spheroidal harmonics. We finish with a summary of our results and conclusions, in section 6.

JHEP03(2007)019

2. Fermion field in a brane-induced rotating black hole background

We start our analysis by presenting the line-element that describes the 4-dimensional gravitational background on a brane placed in the vicinity of a higher-dimensional rotating, uncharged black hole. The latter $(4+n)$-dimensional spacetime is given by the well-known Myers-Perry solution [30]. The induced-on-the-brane gravitational background follows by projecting the higher-dimensional one on the brane, by fixing the values of all additional

azimuthal coordinates to $\pi/2$. Then, the brane line-element assumes the form[1] [7]

$$ds^2 = \Big(1-\frac{\mu}{\Sigma\, r^{n-1}}\Big)dt^2+\frac{2a\mu\sin^2\theta}{\Sigma\, r^{n-1}}\,dt\,d\varphi-\frac{\Sigma}{\Delta}dr^2-\Sigma\,d\theta^2-\Big(r^2+a^2+\frac{a^2\mu\sin^2\theta}{\Sigma\, r^{n-1}}\Big)\sin^2\theta\,d\varphi^2\,, \tag{2.1}$$

where

$$\Delta = r^2+a^2-\frac{\mu}{r^{n-1}}\,, \qquad \Sigma = r^2+a^2\,\cos^2\theta\,. \tag{2.2}$$

The mass and angular momentum (transverse to the $r\varphi$-plane) of the black hole are then given by

$$M_{\rm BH} = \frac{(n+2)A_{n+2}}{16\pi G}\,\mu\,, \qquad J = \frac{2}{n+2}\,M_{\rm BH}\,a\,, \tag{2.3}$$

with G being the $(4+n)$-dimensional Newton's constant, and A_{n+2} the area of an $(n+2)$-dimensional unit sphere, given by

$$A_{n+2} = \frac{2\pi^{(n+3)/2}}{\Gamma[(n+3)/2]}\,. \tag{2.4}$$

The 4-dimensional background (2.1) is the one 'felt' by all Standard Model fields, including fermions, which are restricted to live on the brane. As the reader notes, the higher-dimensional black hole has been assumed to have only one angular momentum component, instead of the $[(n+3)/2]$ possible ones. The reason for this is that, under the assumption that the brane is infinitely-thin, the colliding particles have a non-vanishing impact parameter only along the usual three spacelike coordinates; therefore, the resulting angular momentum will be around an axis also in our brane. An upper bound can be imposed on this sole angular momentum parameter of the black hole by demanding the creation of the black hole from the collision of the two particles. The maximum value of the impact parameter between the two particles that can lead to the creation of a black hole was found to be [9]

$$b_{\rm max} = 2\left[1+\left(\frac{n+2}{2}\right)^2\right]^{-\frac{1}{(n+1)}}\mu^{\frac{1}{(n+1)}}\,. \tag{2.5}$$

This, in conjunction with the relation $J = bM_{\rm BH}/2$ [22] for the angular momentum of the black hole, leads to

$$a_*^{\rm max} = \frac{n+2}{2}\,, \tag{2.6}$$

where $a_* \equiv a/r_h$. For $n \geq 1$, the black hole horizon is given by the unique solution of the equation $\Delta(r) = 0$, and may be conveniently written as $r_h^{n+1} = \mu/(1+a_*^2)$.

Using the Newman-Penrose formalism, the Kinnersley tetrad and Boyer-Lindquist coordinates, Teukolsky [33] decoupled the field equations for spin $s = 0, 1/2, 1$ and 2 field perturbations of a Petrov Type D (vacuum) background metric (that also includes the

[1] In order for the black hole to be considered a classical object, its mass $M_{\rm BH}$ will be assumed to be at least a few times larger than the fundamental scale of gravity M_*. Then, under the assumption that the brane self-energy is of the order of M_*, its effect on the gravitational background can be considered negligible. Analyses that address the complete bulk-brane-black-hole system have only led, up to now, to consistent brane trajectories solutions [31] — for an attempt to analytically construct a small black hole stuck on a tensional brane, see [32].

JHEP03(2007)019

traditional 4-dimensional Kerr spacetime). Teukolsky expressed all the spin-field equations as one single 'master' equation, with the 'helicity', or spin-weight, $h = (+|s|, -|s|)$ of the field as a parameter. As Teukolsky's original equation does not apply to the case of propagation in a projected-on-the-brane higher-dimensional background, as the one given in eq. (2.1), here we have re-derived this equation. The new 'brane master' equation now describes spin $s = 0, 1/2$ and 1 field perturbations of both 'helicities', and has the form

$$\left[\frac{(r^2+a^2)^2}{\Delta} - a^2\sin^2\theta\right]\frac{\partial^2\Omega_h}{\partial t^2} + \frac{2a\mu}{\Delta r^{n-1}}\frac{\partial^2\Omega_h}{\partial t\,\partial\phi} + \left[\frac{a^2}{\Delta} - \frac{1}{\sin^2\theta}\right]\frac{\partial^2\Omega_h}{\partial\phi^2} - \tag{2.7}$$
$$\Delta^{-h}\frac{\partial}{\partial r}\left(\Delta^{h+1}\frac{\partial\Omega_h}{\partial r}\right) - \frac{1}{\sin\theta}\frac{\partial}{\partial\theta}\left(\sin\theta\frac{\partial\Omega_h}{\partial\theta}\right) - 2h\left[\frac{a\Delta'(r)}{2\Delta} + \frac{i\cos\theta}{\sin^2\theta}\right]\frac{\partial\Omega_h}{\partial\phi} +$$
$$2h\left[r + \bar{\rho} - \frac{(r^2+a^2)\Delta'(r)}{2\Delta}\right]\frac{\partial\Omega_h}{\partial t} + h\left[h\cot^2\theta - 1 + (2-\Delta''(r))\delta_{h,|h|}\right]\Omega_h = \Sigma\cdot T_h\,,$$

where $\bar{\rho} = r + ia\cos\theta$. In the above, $\Omega_h = \Omega_h(t, r, \theta, \phi)$ represents the spin-field perturbation and T_h the source term in the field equations - we refer the reader to [7, 33] for details on the derivation of the above equation, and for the precise definitions of $\Omega_h(t, r, \theta, \phi)$ and T_h, in each spin case. Equation (2.7) is formally the same as Teukolsky's original four-dimensional equation, except for the different expression of the metric function $\Delta(r)$ which is now n-dependent, and the term with $\Delta''(r)$ which is identically zero in four dimensions (this was already noted in [25] for the spin-1 case) and, obviously, for $h < 0$.

The 'master' equation (2.7) is clearly separable for any value of the 'helicity' h, so that its solution can be written as a sum over the Fourier modes:

$$\Omega_h(t, r, \theta, \phi) = \int_{-\infty}^{+\infty} d\omega \sum_{l=|h|}^{+\infty}\sum_{m=-l}^{+l} {}_h a_\Lambda\ {}_h\Omega_\Lambda(t, r, \theta, \phi) \tag{2.8}$$
$${}_h\Omega_\Lambda(t, r, \theta, \phi) = {}_hR_\Lambda(r)\,{}_hS_\Lambda(\theta)e^{-i\omega t}e^{+im\phi}\,,$$

where ${}_h a_\Lambda$ are the Fourier coefficients, and the set of 'quantum' numbers is denoted by $\Lambda \equiv \{\ell m\omega\}$.

The radial and angular ODEs resulting from the separation of variables of the 'master' equation are, respectively:

$$\Delta^{-h}\frac{d}{dr}\left(\Delta^{h+1}\frac{d_hR_\Lambda}{dr}\right) + \left[\frac{K^2 - ihK\Delta'(r)}{\Delta} + 4ih\omega r + h(\Delta''(r)-2)\delta_{h,|h|} - {}_h\lambda_\Lambda\right]{}_hR_\Lambda = 0 \tag{2.9}$$

where we have used the definition

$$K = (r^2+a^2)\omega - am, \tag{2.10}$$

and

$$\left[\frac{d}{dx}\left((1-x^2)\frac{d}{dx}\right) + a^2\omega^2(x^2-1) - 2ha\omega x - \frac{(m+hx)^2}{1-x^2} + {}_h\lambda_\Lambda + 2ma\omega + h\right]{}_hS_\Lambda(x) = 0\,, \tag{2.11}$$

where $x \equiv \cos\theta$. In the above, ${}_h\lambda_\Lambda$ is the constant of separation between the angular and radial equations.

In the spin-1/2 case, the wave function of the fermion is represented by two spinors P^A and $\bar{Q}^{A'}$ [34], that, in the massless case, satisfy the equations $\nabla_{AA'}P^A = \nabla_{AA'}Q^A = 0$. By using the Kinnersley tetrad $(\ell_\mu, n_\mu, m_\mu, m^*_\mu)$ and the Fourier decomposition (2.8), these equations can be separated into first-order ODEs with respect to the θ and r coordinates. For the 2-component spinor $P^A = (P^0, P^1)$, we make the decomposition

$$P^0 = (r - ia\cos\theta)^{-1}\,{}_{-1/2}R_\Lambda(r)\;{}_{-1/2}S_\Lambda(\theta)\,e^{im\phi}e^{-i\omega t} \tag{2.12}$$

$$P^1 = {}_{+1/2}R_\Lambda(r)\;{}_{+1/2}S_\Lambda(\theta)\,e^{im\phi}e^{-i\omega t}. \tag{2.13}$$

Defining new radial functions

$$P_+ = \Delta^{1/2}\,{}_{+1/2}R_\Lambda, \qquad P_- = {}_{-1/2}R_\Lambda\,, \tag{2.14}$$

the first-order radial equations take the form [34]

$$\begin{aligned}\Delta^{1/2}\,(\partial_r - iK/\Delta)\,P_- &= \lambda P_+,\\ \Delta^{1/2}\,(\partial_r + iK/\Delta)\,P_+ &= \lambda P_-,\end{aligned} \tag{2.15}$$

where $\lambda = \sqrt{{}_{-1/2}\lambda_\Lambda}$. It may easily be shown that similar definitions for the components of the $\bar{Q}^{A'}$ spinor lead to the same system of first-order radial ODEs. The coupled radial equations (2.15) may then be written in matrix form as follows

$$\frac{d\mathbf{P}}{dr} = \left(\frac{iK}{\Delta}\boldsymbol{\sigma}_3 + \frac{\lambda}{\Delta^{1/2}}\boldsymbol{\sigma}_1\right)\mathbf{P}\,, \tag{2.16}$$

where $\mathbf{P} = \begin{pmatrix} P_- \\ P_+ \end{pmatrix}$, and $\boldsymbol{\sigma}_1 = \left(\begin{smallmatrix} 0 & 1 \\ 1 & 0 \end{smallmatrix}\right)$ and $\boldsymbol{\sigma}_3 = \left(\begin{smallmatrix} 1 & 0 \\ 0 & -1 \end{smallmatrix}\right)$ are the Pauli spin matrices. By taking the complex conjugate of this equation it is clear that, if $\mathbf{P}$ is a solution, then so is $\boldsymbol{\sigma}_1\mathbf{P}^*$. This transformation corresponds to time-reversal. On causal grounds we will only admit one set of solutions: those that are ingoing at the horizon. This alternative, but equivalent to eq. (2.9), set of radial equations will be used for the numerical determination of the radial part of the spinor wave function, as we will see in detail in section 4.

3. Hawking radiation in the form of fermion fields

We are interested in the Hawking radiation of an evaporating black hole on the brane, which is described by the ("past") Unruh vacuum $|U^-\rangle$. The quantum field theory of fermions on the Kerr black hole has been extensively studied in the literature [35 – 38], but for ease of reference, we now outline the key features. For more details of the general formalism relating to fermions on curved space-time, see [39], or [40] for a more recent review.

In constructing the state $|U^-\rangle$, it is most straightforward to use Dirac 4-spinors, in which case the wavefunction of the massless fermionic field (that, for historical reasons, we call 'neutrino') takes the form [35 – 37]

$$\psi = \frac{e^{-i\omega t}e^{im\varphi}}{\mathcal{F}}\begin{pmatrix}\eta \\ L\eta\end{pmatrix}, \tag{3.1}$$

where

$$\mathcal{F} = \left[\Delta \sin^2\theta\ \bar{\rho}^2\right]^{\frac{1}{4}}. \tag{3.2}$$

Here L is the lepton number [37], so that $L = +1$ for neutrinos and $L = -1$ for anti-neutrinos. The two-spinor η takes the form [35 – 37]

$$\eta = \begin{pmatrix} R_1(r)S_1(\theta) \\ R_2(r)S_2(\theta) \end{pmatrix}. \tag{3.3}$$

The angular functions S_1 and S_2 satisfy the equations [35 – 37]

$$\left[\frac{d}{d\theta} + \left(a\omega\sin\theta - \frac{m}{\sin\theta}\right)\right] S_1(\theta) = \lambda S_2(\theta), \tag{3.4}$$

$$\left[\frac{d}{d\theta} - \left(a\omega\sin\theta - \frac{m}{\sin\theta}\right)\right] S_2(\theta) = -\lambda S_1(\theta), \tag{3.5}$$

and are related to the spin-weighted spheroidal harmonics ${}_hS_\Lambda$ (2.11) by [35]

$$S_1(\theta) = \left(\frac{\sin\theta}{2}\right)^{\frac{1}{2}} {}_{-\frac{1}{2}}S_\Lambda(\cos\theta), \qquad S_2(\theta) = \left(\frac{\sin\theta}{2}\right)^{\frac{1}{2}} {}_{\frac{1}{2}}S_\Lambda(\cos\theta). \tag{3.6}$$

There is a subtlety in the definition of the radial functions R_1, R_2, depending on whether we are considering neutrinos or anti-neutrinos. For neutrinos ($L = +1$), we have [35 – 37]

$$R_1(r) = P_-, \qquad R_2(r) = P_+, \tag{3.7}$$

but for anti-neutrinos ($L = -1$), the radial functions swap over [37]:

$$R_1(r) = P_+, \qquad R_2(r) = P_-. \tag{3.8}$$

This is particularly important when calculating the particle fluxes for neutrinos and anti-neutrinos.

The usual "in" and "up" modes are defined by the behaviour of the radial functions near the horizon and at infinity [35, 36]:

$$\left(P_-^{\rm in}, P_+^{\rm in}\right) = \frac{1}{\sqrt{8\pi^2}} \begin{cases} \left(A_\Lambda^{\rm in} e^{i\omega r_*}, e^{-i\omega r_*}\right) & r \to \infty, \\ \left(0, B_\Lambda^{\rm in} e^{-i\tilde{\omega} r_*}\right) & r \to r_h, \end{cases} \tag{3.9}$$

$$\left(P_-^{\rm up}, P_+^{\rm up}\right) = \frac{1}{\sqrt{8\pi^2}} \begin{cases} \left(B_\Lambda^{\rm up} e^{i\omega r_*}, 0\right) & r \to \infty, \\ \left(e^{i\tilde{\omega} r_*}, A_\Lambda^{\rm up} e^{-i\tilde{\omega} r_*}\right) & r \to r_h, \end{cases} \tag{3.10}$$

and correspond to modes originating either at past infinity or past horizon, respectively. In the above, r_* is the standard "tortoise" co-ordinate, defined by

$$\frac{dr_*}{dr} = \frac{r^2 + a^2}{\Delta(r)}, \tag{3.11}$$

and

$$\tilde{\omega} = \omega - m\Omega, \tag{3.12}$$

with Ω the horizon angular velocity

$$\Omega = \frac{a_*}{(1+a_*^2)\, r_h}. \tag{3.13}$$

In eqs. (3.9)–(3.10), $A_\Lambda^{\rm in}$, $B_\Lambda^{\rm in}$, $A_\Lambda^{\rm up}$, $B_\Lambda^{\rm up}$ are constants of integration which satisfy the Wronskian relations [36]

$$1 - |A_\Lambda^\bullet|^2 = |B_\Lambda^\bullet|^2\,, \qquad B_\Lambda^{\rm up^*} = -B_\Lambda^{\rm in}, \tag{3.14}$$

where $\bullet$ is either "in" or "up". These relations are useful for simplifying the flux formulae we shall derive in this section.

The ("past") Unruh vacuum $|U^-\rangle$ is defined in the usual way, by taking the "in" modes to have positive frequency with respect to co-ordinate time near infinity (which corresponds to $\omega > 0$) and using a set of modes having positive frequency with respect to Kruskal time in the vicinity of the past event horizon. Using the lemma in appendix H of [41], a suitable set of modes having positive frequency with respect to Kruskal time near the past horizon is

$$\left[2\cosh\left(\frac{\tilde\omega}{2T_{\rm H}}\right)\right]^{-\frac{1}{2}} \left\{\exp\left(\frac{\tilde\omega}{4T_{\rm H}}\right)\psi_\Lambda^{\rm up} + \exp\left(\frac{-\tilde\omega}{4T_{\rm H}}\right)\psi_\Lambda^{\rm down^*}\right\}, \tag{3.15}$$

for *any* value of $\tilde\omega$. The modes $\psi_\Lambda^{\rm down}$ are given by the complex conjugate of the modes $\psi_\Lambda^{\rm up}$, after changing the sign of the Kruskal co-ordinates. Similarly, a suitable set of modes having *negative* frequency with respect to Kruskal time near the past horizon is

$$\left[2\cosh\left(\frac{\tilde\omega}{2T_{\rm H}}\right)\right]^{-\frac{1}{2}} \left\{\exp\left(\frac{-\tilde\omega}{4T_{\rm H}}\right)\psi_\Lambda^{\rm up} + \exp\left(\frac{\tilde\omega}{4T_{\rm H}}\right)\psi_\Lambda^{\rm down^*}\right\}, \tag{3.16}$$

for any value of $\tilde\omega$. The "down" modes are vanishing on the right-hand quadrant of the conformal diagram of the space-time, which is the region in which we are interested. Therefore we do not consider them further. Further details of this construction can be found in [35, 41, 42]. We therefore find that a suitable expansion for the neutrino field in terms of our positive and negative frequency modes is (cf. [35]):

$$\begin{aligned}\Psi = \sum_{\ell=1/2}^{\infty}\sum_{m=-\ell}^{\ell}\Bigg\{&\int_{\omega>0} d\omega\left[\psi_\Lambda^{\rm in}\hat a_\Lambda^{\rm in} + \psi_{-\Lambda}^{\rm in^*}\hat b_\Lambda^{\rm in\dagger}\right] \\ &+ \int_{{\rm all}\,\tilde\omega} d\tilde\omega\left[2\cosh\left(\frac{\tilde\omega}{2T_H}\right)\right]^{-\frac{1}{2}}\left[\exp\left(\frac{\tilde\omega}{4T_H}\right)\hat a_\Lambda^{\rm up} + \exp\left(\frac{-\tilde\omega}{4T_H}\right)\hat b_\Lambda^{\rm up\dagger}\right]\psi_\Lambda^{\rm up}\Bigg\},\end{aligned} \tag{3.17}$$

where $-\Lambda \equiv \{\ell, -m, -\omega\}$ and $T_{\rm H}$ is the Hawking temperature of the $(4+n)$-dimensional, rotating black hole, given by

$$T_{\rm H} = \frac{(n+1) + (n-1)\, a_*^2}{4\pi\,(1+a_*^2)\, r_h}\,. \tag{3.18}$$

The Fourier coefficients ${}_h a_\Lambda$ in (2.8) have been promoted to quantum operators $\hat a_\Lambda$ (where we have dropped the helicity subindex h for clarity). The state $|U^-\rangle$ is then annihilated by the operators $\hat a_\Lambda^\bullet$ and $\hat b_\Lambda^\bullet$:

$$\hat a_\Lambda^{\rm in}\left|U^-\right\rangle = \hat a_\Lambda^{\rm up}\left|U^-\right\rangle = 0 = \hat b_\Lambda^{\rm in}\left|U^-\right\rangle = \hat b_\Lambda^{\rm up}\left|U^-\right\rangle. \tag{3.19}$$

We now have the machinery in place to compute the fluxes of particles, energy and angular momentum from the black hole.

Firstly, the particle flux is given by [35, 36]

$$\frac{dN}{dt} = \int_{S_\infty} d\theta\, d\varphi\, r^2 \sin\theta\, \langle U^-|J^r|U^-\rangle\,, \tag{3.20}$$

where J^r is the radial component of the conserved current [36]:

$$J^\mu = \frac{1}{2}\left[\bar{\Psi}, \gamma^\mu \Psi\right]. \tag{3.21}$$

Here, the Dirac adjoint $\bar{\Psi}$ is defined by [36, 39]:

$$\bar{\Psi} = \Psi^\dagger \gamma^0, \tag{3.22}$$

where γ^0 is the flat-space Dirac matrix. A suitable representation of the curved-space Dirac matrices γ^μ for the space-time metric (2.1) can be found in [36]. We compute the fluxes for neutrinos ν and antineutrinos $\bar{\nu}$, using the field expansion (3.17) and the mode functions of the form (3.1). This gives the total particle flux per unit time to be [35]:

$$\frac{d^2 N_{\nu+\bar{\nu}}}{d(\cos\theta)dt} = \frac{1}{4\pi}\sum_{\ell=1/2}^{\infty}\sum_{m=-\ell}^{\ell}\int_{\omega=0}^{\infty}\frac{d\omega}{\exp\left(\tilde{\omega}/T_{\rm H}\right)+1}\mathbb{T}_\Lambda\left({}_{-1/2}S_\Lambda^2 + {}_{+1/2}S_\Lambda^2\right). \tag{3.23}$$

The transmission coefficient $\mathbb{T}_\Lambda$ is the transmitted proportion of the flux which, in the case of an "up" mode (3.10) is equal to

$$\mathbb{T}_\Lambda = \left|B_\Lambda^{\rm up}\right|^2. \tag{3.24}$$

By virtue of the Wronskian relations (3.14) this is the same as the absorption probability of an "in" mode. Similarly, the net particle flux is [35]

$$\frac{d^2 N_{\nu-\bar{\nu}}}{d(\cos\theta)dt} = \frac{1}{4\pi}\sum_{\ell=1/2}^{\infty}\sum_{m=-\ell}^{\ell}\int_{\omega=0}^{\infty}\frac{d\omega}{\exp\left(\tilde{\omega}/T_{\rm H}\right)+1}\mathbb{T}_\Lambda\left({}_{-1/2}S_\Lambda^2 - {}_{+1/2}S_\Lambda^2\right). \tag{3.25}$$

It is tempting, in view of eqs. (3.23) and (3.25) to view the contribution from neutrinos as being proportional to ${}_{-1/2}S_\Lambda$ and that from anti-neutrinos as being proportional to ${}_{+1/2}S_\Lambda$. In fact, at infinity, this is the case, but only because of the form of the "in" and "up" modes in this limit and eqs. (3.7)–(3.8). It is not true more generally.

The fluxes of energy and angular momentum per unit time are given in terms of components of the stress-energy tensor:

$$\frac{dE}{dt} = \int_{S_\infty} d\theta\, d\varphi\, r^2 \sin\theta\, \langle U^-|T^{tr}|U^-\rangle, \tag{3.26}$$

$$\frac{dJ}{dt} = \int_{S_\infty} d\theta\, d\varphi\, r^2 \sin\theta\, \langle U^-|T^r_\varphi|U^-\rangle\,, \tag{3.27}$$

JHEP03(2007)019

where the stress-energy tensor of the neutrino field is given by [36]

$$T_{\mu\nu} = \frac{i}{4}\Big(\big[\bar{\Psi}, \gamma_{(\mu}\nabla_{\nu)}\Psi\big] - \big[\nabla_{(\mu}\bar{\Psi}, \gamma_{\nu)}\Psi\big] \Big). \tag{3.28}$$

The spinor covariant derivative is defined by [36]

$$\nabla_\mu \Psi = (\partial_\mu - \Gamma_\mu)\,\Psi, \tag{3.29}$$

where the Γ_μ matrices can be taken to be traceless and satisfy [36]

$$\gamma^\mu{}_{;\nu} - \Gamma_\nu \gamma^\mu + \gamma^\mu \Gamma_\nu = 0. \tag{3.30}$$

These can be straightforwardly computed using the formula (cf. [43], but with different conventions)

$$\Gamma_\mu = -\frac{1}{8} g_{\nu\sigma}\left[\gamma^\sigma, \gamma^\nu{}_{;\mu}\right]. \tag{3.31}$$

The formulae for the matrices Γ_μ are sufficiently large that we do not reproduce them here.

After computing the expectation value of the stress-energy tensor in the state $|U^-\rangle$, the total fluxes of particles, energy and angular momentum emitted by the black hole per unit time and frequency, in the form of fermion modes, are given by [35]

$$\frac{d^2 N_{\nu+\bar{\nu}}}{dt d\omega} = \frac{1}{2\pi}\sum_{\ell=1/2}^{\infty}\sum_{m=-\ell}^{\ell} \frac{1}{\exp\left(\tilde{\omega}/T_{\rm H}\right)+1}\mathbb{T}_\Lambda\,, \tag{3.32}$$

$$\frac{d^2 E}{dt d\omega} = \frac{1}{2\pi}\sum_{\ell=1/2}^{\infty}\sum_{m=-\ell}^{\ell} \frac{\omega}{\exp\left(\tilde{\omega}/T_{\rm H}\right)+1}\mathbb{T}_\Lambda\,, \tag{3.33}$$

$$\frac{d^2 J}{dt d\omega} = \frac{1}{2\pi}\sum_{\ell=1/2}^{\infty}\sum_{m=-\ell}^{\ell} \frac{m}{\exp\left(\tilde{\omega}/T_{\rm H}\right)+1}\mathbb{T}_\Lambda\,. \tag{3.34}$$

The emission rates (3.32)–(3.34) describe the different fluxes emitted by the black hole over the whole solid angle $\Omega_2^2 = 4\pi$, and follow by performing an integration over the angular coordinates θ and ϕ. If we go one step backwards, we may derive the angular distribution of the emitted radiation by displaying the exact dependence of the differential rates on the azimuthal angle θ, and write

$$\frac{d^3 N_{\nu+\bar{\nu}}}{d(\cos\theta) dt d\omega} = \frac{1}{4\pi}\sum_{\ell=1/2}^{\infty}\sum_{m=-\ell}^{\ell} \frac{1}{\exp\left(\tilde{\omega}/T_{\rm H}\right)+1}\mathbb{T}_\Lambda\left({}_{-1/2}S_\Lambda^2 + {}_{+1/2}S_\Lambda^2\right), \tag{3.35}$$

$$\frac{d^3 E}{d(\cos\theta) dt d\omega} = \frac{1}{4\pi}\sum_{\ell=1/2}^{\infty}\sum_{m=-\ell}^{\ell} \frac{\omega}{\exp\left(\tilde{\omega}/T_{\rm H}\right)+1}\mathbb{T}_\Lambda\left({}_{-1/2}S_\Lambda^2 + {}_{+1/2}S_\Lambda^2\right). \tag{3.36}$$

It is easy to check that the above two expressions reduce to eqs. (3.32)–(3.33) when we use the angular function normalization

$$\int_{-1}^{1} \left|{}_{\pm 1/2}S_\Lambda(\cos\theta)\right|^2 d(\cos\theta) = \int_{-1}^{1} \left|{}_{\pm 1/2}S_\Lambda(x)\right|^2 dx = 1\,. \tag{3.37}$$

Note that in the particle (3.35) and power (3.36) fluxes, both 'helicities' $h = -1/2$ and $h = +1/2$ make a contribution. As we will see, this will lead to radiation spectra that are invariant under the parity transformation $\theta \to \pi - \theta$ (for more discussions on the asymmetry under parity of the derived spectra in purely four dimensions, see, e.g. [35, 37, 38]).

4. Numerical analysis

The transmitted flux in each angular mode may be calculated by numerically solving the radial equations. Before we may begin, however, we must first solve the angular equations to determine the eigenvalue $\lambda = \sqrt{{}_{-1/2}\lambda_\Lambda}$ that appears in the radial equations. In order to compute the angular distributions of the particle and energy fluxes, we will also need the angular eigenvectors: the spin-1/2-weighted spheroidal harmonics. In this section, we briefly outline the numerical methods used to solve both the angular and radial equations, and describe our method for determining the transmission coefficient $\mathbb{T}_\Lambda$.

The angular eigenvalues ${}_h\lambda_\Lambda$ were calculated using a spectral decomposition method, described in a paper by Hughes [44]. In appendix A of [44], it is shown that spheroidal harmonics may be expanded as a sum over spherical harmonics of the same spin-weight,

$$ {}_hS_\Lambda(\theta) = \sum_{j=l_{\min}}^{\infty} {}_hb_{lj}^{a\omega}\, {}_hY_{jm}(\theta)\,, \tag{4.1} $$

where $l_{\min} = \max(|h|, |m|)$. A recurrence relation for the expansion coefficients ${}_hb_{lj}^{a\omega}$ is generated by substituting (4.1) into the angular equation (2.11) and exploiting the orthogonality properties of the spin-weighted spherical harmonics. Writing $b_j \equiv {}_hb_{lj}^{a\omega}$ for clarity, the result is

$$ \begin{aligned} -\,{}_h\mathcal{E}_{jm\omega}\, b_j \;=\; & \left[(a\omega)^2 c^m_{j-2,j,2}\right] b_{j-2} + \left[(a\omega)^2 c^m_{j-1,j,2} - 2a\omega h c^m_{j-1,j,1}\right] b_{j-1} \\ & + \left[(a\omega)^2 c^m_{j,j,2} - 2a\omega h c^m_{j,j,1} - j(j+1)\right] b_j \\ & + \left[(a\omega)^2 c^m_{j+1,j,2} - 2a\omega h c^m_{j+1,j,1}\right] b_{j+1} + \left[(a\omega)^2 c^m_{j+2,j,2}\right] b_{j+2}, \end{aligned} \tag{4.2} $$

where we have defined

$$ c^m_{j,l,2} = \frac{2}{3}\sqrt{\frac{2j+1}{2l+1}}\langle j, 2, m, 0 | l, m\rangle \langle j, 2, -h, 0 | l, -h\rangle + \frac{1}{3}\delta_{jl}, \tag{4.3} $$

$$ c^m_{j,l,1} = \sqrt{\frac{2j+1}{2l+1}}\langle j, 1, m, 0 | l, m\rangle \langle j, 1, -h, 0 | l, -h\rangle. \tag{4.4} $$

Here, $\langle j, i, m, 0 | l, n\rangle$ are Clebsch-Gordan coefficients. The separation constant ${}_h\mathcal{E}_\Lambda$, appearing on the left-hand-side of eq. (4.2), is related to the angular parameter ${}_h\lambda_\Lambda$ by

$$ {}_h\mathcal{E}_\Lambda = {}_h\lambda_\Lambda + 2ma\omega - a^2\omega^2 + h(h+1). \tag{4.5} $$

In the spin-half case, ℓ and m are half-integers, and $h = -1/2$. In the non-rotating limit the solution reduces to $\mathcal{E}_{\ell m} = \ell(\ell+1)$ and ${}_{-1/2}\lambda_\Lambda = (\ell + \frac{1}{2})^2$.

The recurrence relations (4.2) may be rewritten in matrix form. The eigenvalue of the matrix is (minus) the separation constant ${}_h\mathcal{E}_\Lambda$, and the eigenvector is a column of expansion

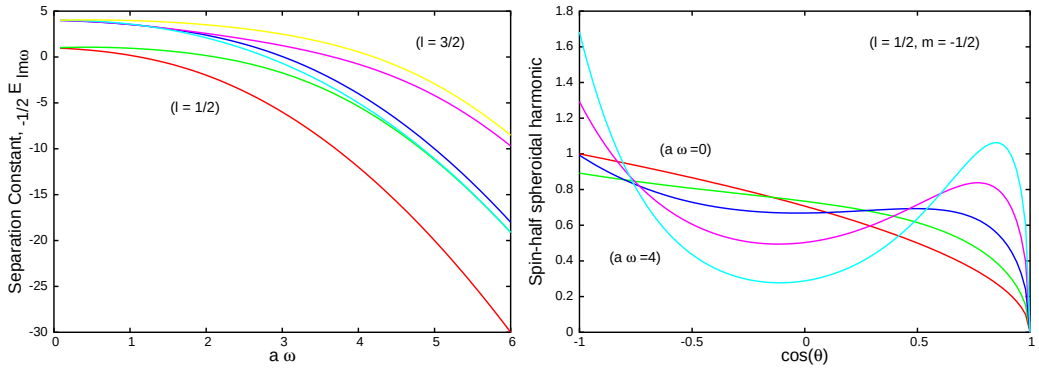

Figure 1: **(a)** The separation constant ${}_h\mathcal{E}_\Lambda$, for the modes $\ell = 1/2, 3/2$ and $m = -\ell, \ldots, \ell$, and 'helicity' $h = -1/2$; **(b)** Spin-1/2 weighted spheroidal harmonics for a spinor field with $h = -1/2$, $\ell = 1/2$, $m = -1/2$, and for $a\omega = (0, 1, 2, 3, 4)$.

coefficients b_j. Since the matrix is band-diagonal, the eigenproblem may be solved in a numerically efficient way. For more details on this method, see appendix A in [44].

The results for the angular eigenvalues were independently checked using a partial fraction method [45], and a variant of the 'shooting' method [46], which is described in detail in [25, 47]. The angular eigenvalues coincided up to double precision. The values of the corresponding separation constants ${}_h\mathcal{E}_\Lambda$ following from the above analysis are shown in figure 1(a), for some indicative spin-1/2 modes.

The spectral decomposition method may also be used to calculate the angular functions ${}_hS_\Lambda(x)$, according to eq. (4.1). However, this calculation would first require the determination of the spin-weighted spherical harmonics ${}_hY_{jm}(\theta)$. Instead, we preferred to follow the series expansion approach introduced by Leaver [45]. A solution to eq. (2.11) may be expressed as

$$ {}_hS_\Lambda(x) = e^{a\omega x}(1+x)^{\frac{1}{2}|m-h|}(1-x)^{\frac{1}{2}|m+h|}\sum_{n=0}^{\infty} c_n(1+x)^n, \tag{4.6} $$

where $x = \cos(\theta)$ and the expansion coefficients c_n are related by a three-term recurrence relation,

$$ \alpha_0 c_1 + \beta_0 c_0 = 0, \tag{4.7} $$

$$ \alpha_n c_{n+1} + \beta_n c_n + \gamma_n c_{n-1} = 0, \quad n = 1, 2, \ldots \tag{4.8} $$

The recurrence coefficients $\alpha_n, \beta_n, \gamma_n$ are

$$ \begin{aligned} \alpha_n &= -2(n+1)(n+2k_-+1) \\ \beta_n &= n(n-1) + 2n(k_- + k_+ + 1 - 2a\omega) \\ &\quad - [2a\omega(2k_- + h + 1) - (k_- + k_+)(k_- + k_+ + 1)] - \left[a^2\omega^2 + {}_h\mathcal{E}_\Lambda\right] \\ \gamma_n &= 2a\omega(n + k_- + k_+ + h), \end{aligned} \tag{4.9} $$

with $k_- = \frac{1}{2}|m-h|$ and $k_+ = \frac{1}{2}|m+h|$. This expansion, together with the eigenvalue ${}_h\mathcal{E}_\Lambda$ calculated via the spectral decomposition, provides an efficient method for the calculation of spin-half spheroidal harmonics, such as those shown in figure 1(b). Note that ${}_{-1/2}S^2_\Lambda$ is clearly greater on the Southern hemisphere than on the Northern one, with a similar (but opposite) asymmetry arising also for ${}_{+1/2}S^2_\Lambda$. However, their sum is invariant under the change $\theta \to \pi - \theta$, which means that, unless both 'helicities' $h = \pm 1/2$ are taken into account in the calculation of the angular distribution of the radiation fluxes (3.35) and (3.36), the resulting fermionic emission will be asymmetric with respect to parity.

Once the eigenvalues of the angular equation are known, we may proceed to solve the radial equations. One possible approach is to start from the second-order radial Teukolsky equation (2.9), and introduce a new radial "tortoise" coordinate (like the one in (3.11)) to transform to a potential barrier problem

$$\left[\frac{d^2}{dr_*{}^2} - V(r)\right] R(r) = 0. \tag{4.10}$$

Equations of this form are familiar from quantum mechanical problems, and standard methods for finding transmission coefficients may be employed. However, a disadvantage of this method is that the definition of the tortoise coordinate depends on the number of extra dimensions, and the relation $r_*(r)$ can be hard to invert (see the discussion in [25]). Here, we prefer instead to work with the pair of coupled first-order equations (2.16). These may be solved by combining series expansions at the horizon and at infinity with numerical integration, as described below.

Briefly, our method for determining the transmission coefficient $\mathbb{T}_\Lambda$ is as follows. We start by demanding that the solution be purely ingoing at the horizon. The ingoing solution may be written as a power series in $(r/r_h - 1)^{1/2}$ (see next subsection). We evaluate this series solution at tenth order at a point close to the horizon ($r/r_h - 1 \leq 10^{-4}$) and use this as the initial condition for a numerical integration scheme. We integrate outwards into the asymptotically-flat region, $r/r_h \geq 100$, using a fourth-order Runge-Kutta routine. Here, the solution is matched onto ingoing and outgoing power series solutions in r_h/r which are also evaluated at tenth order. The asymptotic solution at infinity is a linear sum of ingoing and outgoing waves,

$$\mathbf{P} \to A^{\rm in}\,\mathbf{P}^{\rm in} + A^{\rm out}\,\mathbf{P}^{\rm out}, \qquad \text{as } r \to +\infty, \tag{4.11}$$

where $A^{\rm in}$ and $A^{\rm out}$ are complex constants, and $\mathbf{P}^{\rm in}$ and $\mathbf{P}^{\rm out} = \boldsymbol{\sigma}_1 \mathbf{P}^{\rm in *}$ are series expansions described below. Using our numerical solution we may determine $A^{\rm in}$ and $A^{\rm out}$ up to an overall magnitude and phase. The transmission coefficient is then simply

$$\mathbb{T}_\Lambda = 1 - \left|\frac{A^{\rm out}}{A^{\rm in}}\right|^2. \tag{4.12}$$

4.1 Expansion at the horizon

We may write K and Δ as power series around $r = r_h$,

$$K = \sum_{k=0}^{2} K_k \left(\frac{r}{r_h} - 1\right)^k, \qquad\qquad \Delta = \sum_{k=1}^{\infty} \Delta_k \left(\frac{r}{r_h} - 1\right)^k. \tag{4.13}$$

The first terms are

$$K_0 = (r_h^2 + a^2)\omega - am, \qquad K_1 = 2\omega r_h^2, \tag{4.14}$$

$$\Delta_1 = 2r_h^2 + (r_h^2 + a^2)(n-1), \qquad \Delta_2 = r_h^2 - \tfrac{1}{2}n(n-1)(r_h^2 + a^2). \tag{4.15}$$

Defining $\eta \equiv (r/r_h - 1)^{1/2}$, the radial equations (2.16) may be written as

$$\frac{d\mathbf{P}}{d\eta} = \frac{1}{\eta}\,\mathbf{M}(\eta)\,\mathbf{P}, \tag{4.16}$$

where

$$\mathbf{M}(\eta) = \sum_{k=0}^{\infty} \mathbf{M}_k\,\eta^k = (2is_0)\,\boldsymbol{\sigma}_3 + \eta\left(\tfrac{2\lambda r_h}{\sqrt{\Delta_1}}\right)\boldsymbol{\sigma}_1 + \eta^2 2is_0\left(\tfrac{K_1}{K_0} - \tfrac{\Delta_2}{\Delta_1}\right)\boldsymbol{\sigma}_3 + \ldots \tag{4.17}$$

and $s_0 = K_0 r_h/\Delta_1$. This form makes it clear that $r = r_h$ is a regular singular point of the radial equations.

The ingoing solution at the horizon may then be written as

$$\mathbf{P}^{\rm in} = \begin{bmatrix} P_- \\ P_+ \end{bmatrix} = \left(\frac{r}{r_h} - 1\right)^{-is_0} \begin{bmatrix} \frac{2\lambda r_h}{\sqrt{\Delta_1}(1-4is_0)}\,\eta + \ldots \\ 1 + \left(\frac{2\lambda^2 r_h^2}{\Delta_1(1-4is_0)} - is_0\left(\frac{K_1}{K_0} - \frac{\Delta_2}{\Delta_1}\right)\right)\eta^2 + \ldots \end{bmatrix}. \tag{4.18}$$

Note that the P_- series expansion includes only odd powers of η, whereas the P_+ expansion includes only even powers. The outgoing solution may be generated by time-reversal, that is, $\mathbf{P}^{\rm out} = \boldsymbol{\sigma}_1 \mathbf{P}^{\rm in*}$.

4.2 Expansion at infinity

Similar techniques may be applied to find an expansion around the singular point at infinity. First, we define $z \equiv r_h/r$. The radial equations can then be expressed as

$$\frac{d\mathbf{P}}{dz} = \frac{1}{z^2}\left(\sum_{k=0}^{\infty} \mathbf{N}_k\, z^k\right)\mathbf{P}. \tag{4.19}$$

This makes it clear that the point at infinity is an irregular singular point (of rank 1) and we should look for a series expansion of the form

$$\mathbf{P} = e^{t_0 z^{-1}} z^{-t_1} \sum_{k=0}^{\infty} \boldsymbol{\xi}_k\, z^k, \tag{4.20}$$

where t_0 and t_1 are constants, and $\boldsymbol{\xi}_k$ are two-component eigenvectors to be determined. Substituting this into the radial equations and equating the coefficients of like powers of z yields a system of equations

$$(\mathbf{N}_0 + t_0)\boldsymbol{\xi}_0 = 0 \tag{4.21}$$

$$(\mathbf{N}_0 + t_0)\boldsymbol{\xi}_1 = -(\mathbf{N}_1 + t_1)\boldsymbol{\xi}_0 \tag{4.22}$$

$$(\mathbf{N}_0 + t_0)\boldsymbol{\xi}_2 = -(\mathbf{N}_1 + (t_1 - 1))\boldsymbol{\xi}_1 - \mathbf{N}_2\boldsymbol{\xi}_0 \tag{4.23}$$

$$\ldots$$

$$(\mathbf{N}_0 + t_0)\boldsymbol{\xi}_k = -(\mathbf{N}_1 + (t_1 - (k-1))\boldsymbol{\xi}_{k-1} - \sum_{j=0}^{k-2} \mathbf{N}_{k-j}\boldsymbol{\xi}_j. \tag{4.24}$$

The solution for t_0 and t_1 depends on the number of extra dimensions (n). In 4D, we find

$$t_0 = \pm i\omega r_h, \quad t_1 = \pm i\omega(r_h^2 + a^2)/r_h, \tag{4.25}$$

with the positive choice of sign corresponding to an outgoing solution. In 4D such a series solution is given by

$$\begin{aligned} \mathbf{P}^{\rm out} &= \begin{pmatrix} P_- \\ P_+ \end{pmatrix} \\ &= e^{i\omega r} r^{i\omega(r_h^2+a^2)/r_h} \left(\begin{bmatrix} 1 \\ 0 \end{bmatrix} + \frac{i}{2\omega r} \begin{bmatrix} \lambda^2 - 2\omega^2(r_h^2+a^2)^2/r_h^2 + 2a\omega m \\ -\lambda \end{bmatrix} + \mathcal{O}\left(\frac{r_h^2}{r^2}\right) \right). \end{aligned} \tag{4.26}$$

In the asymptotic limit, the upper component dominates over the lower component in the outgoing solution. Again, the ingoing solution can be found by interchanging P_- and P_+ and taking the complex conjugate.

In higher dimensions the index t_0 is unchanged, but $t_1 = 0$. The absence of a logarithmic phase factor for higher-dimensional solutions indicates that the influence of the gravitational potential is now "short-range" for large r (up to $r \sim L$, where L is the size of the extra dimensions). The potential is still "long-range" near the horizon, however, and numerical troubles were avoided by using series expansions at the horizon (and infinity) up to tenth order.

5. Numerical results

In this section, we present exact numerical results for the transmission coefficient and the corresponding particle, energy and angular momentum emission rates for a higher-dimensional, rotating black hole emitting spinor fields on the brane. Their dependence on the dimension of spacetime $n + 4$ and the angular momentum parameter a_* will be investigated, and the angular distribution of the emitted number of particles and energy will also be derived. In the final part of this section, the total emissivities of flux, power and angular momentum will be computed, and their dependence on the fundamental parameters n and a_* will also be discussed.

5.1 Transmission coefficient

The first issue we need to address is the behaviour of the transmission coefficient $\mathbb{T}_\Lambda$ in terms of both the angular momentum parameter a_* and the number of extra dimensions n. The value of $\mathbb{T}_\Lambda$ follows from the numerical integration of the radial equations (2.16) after the exact value of the eigenvalue ${}_h\lambda_\Lambda$ has been determined, as described in the previous section.

The behaviour of the transmission coefficient also strongly depends on the particular mode studied, therefore in figures 2 and 3 we present the dependence of two indicative modes ($\ell = 1/2, m = 1/2$) and ($\ell = 1/2, m = -1/2$) on a_* and n, respectively. Figure 2(a) reveals the monotonic behaviour of $\mathbb{T}_\Lambda$ for modes with $m > 0$ that leads to a continuous enhancement in terms of the angular momentum parameter a_*. On the other hand, as

JHEP03(2007)019

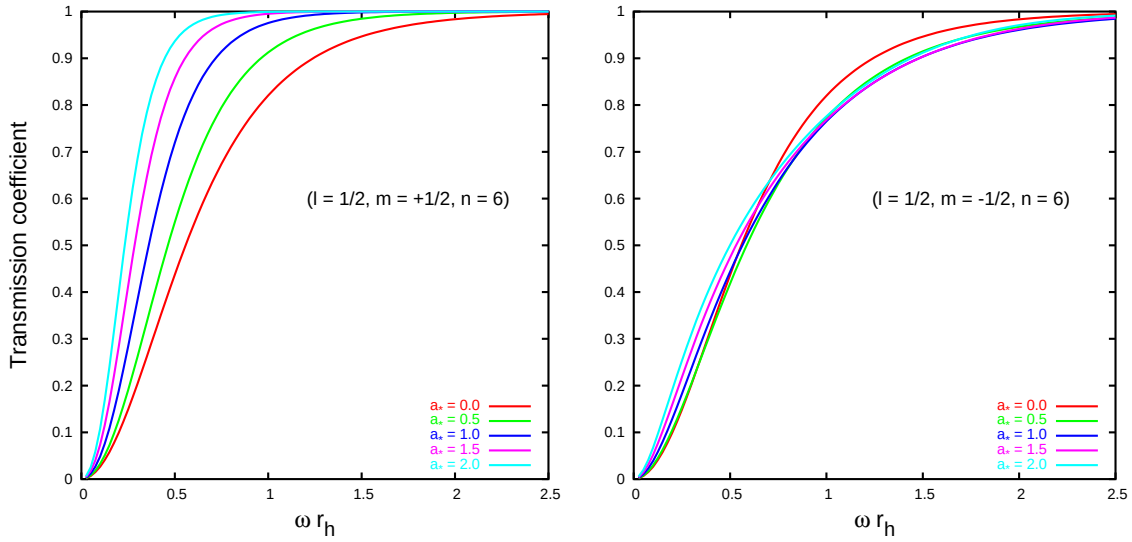

Figure 2: Transmission coefficients for spin-1/2 emission on the brane from a 10-dimensional black hole with variable a_*, for the modes (a) $\ell = 1/2, m = 1/2$, and (b) $\ell = 1/2, m = -1/2$.

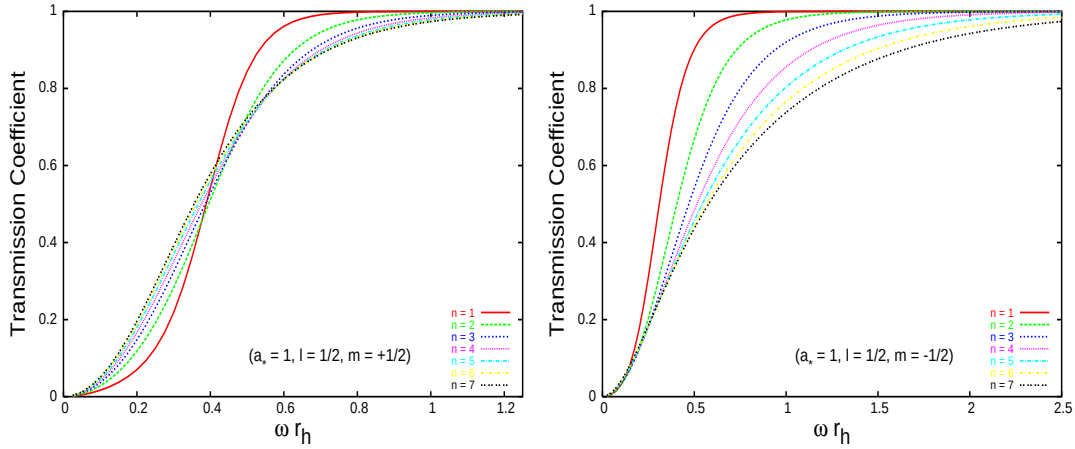

Figure 3: Transmission coefficients for spin-1/2 emission on the brane from a black hole with $a_* = 1$ and variable n, for the modes **(a)** $\ell = 1/2, m = 1/2$, and **(b)** $\ell = 1/2, m = -1/2$.

we may see in figure 2(b), modes with $m < 0$ exhibit a non-monotonic behaviour that strongly depends on the energy regime that is probed: whereas the transmission coefficient is enhanced in the low-energy regime, it is suppressed in the high-energy one. The two panels of figure 3 depict the dependence of $\mathbb{T}_\Lambda$ on the number of the transverse-to-the-brane dimensions n. The exhibited behaviour is again found to be mode- and energy-dependent. Modes with $m < 0$ have a transmission coefficient which is monotonically suppressed with n, while the behaviour of modes with $m > 0$ is characterised by enhancement in the low-energy regime and suppression in the high-energy one.

A similar behaviour in terms of a_* and n was found for the corresponding modes of

JHEP03(2007)019

the emitted gauge bosons studied in [25]. The dependence of modes with $m < 0$ is easily observed to be identical in the two cases. For modes with $m > 0$, though, the agreement is not obvious since, in the case of gauge bosons, modes with $m > 0$ are superradiant ones. Nevertheless, when the fact that a 'more negative' value of $\mathbb{T}_\Lambda$ in the superradiant case is equivalent to a 'more positive' value in the non-superradiant one, agreement is again found between the two cases. In [25], a detailed analysis was performed to show that the above behaviour of the transmission coefficient was directly linked to the behaviour of the effective potential seen by the propagating emitted mode - as the behaviour found for fermions is similar to those for gauge bosons, we will not repeat the same discussion here but, instead, refer the reader to ref. [25] for more information on this point.

The spectrum of the emitted fermionic modes will also be strongly determined by the behaviour of the thermal factor $(e^{\tilde{\omega}/T_{\rm H}} + 1)^{-1}$ in terms of the same parameters n and a_*. It may be easily seen that, for fixed a_* and r_h, the temperature of the black hole increases with the number of extra dimensions n, thus giving a boost to all emission spectra. The dependence on the angular momentum parameter a_*, on the other hand, is much more subtle, and depends on the particular mode and energy regime. For modes with $m < 0$, a simple numerical analysis reveals that the exponent $\tilde{\omega}/T_{\rm H}$ is an increasing function of a_*, for all values of ω, as long as $n \leq 1$, thus leading to a possible suppression of the emission rates for these modes as a_* increases; however, for $n > 1$, this exponent is found to be a decreasing function of a_*, for low enough values of the energy and high enough values of the angular momentum of the black hole. As the transmission coefficient is also enhanced in these regimes, according to figure 2(b), fermionic modes with negative m are more likely to be found in the low-energy part of the spectrum of rapidly rotating black holes. Finally, for modes with $m > 0$, the exponent is found to be a decreasing function of a_* in the low-angular-momentum regime, and an increasing function otherwise, independently of the energy of the mode; as the transmission coefficient is also monotonically enhanced with a_*, we expect these modes to mainly dominate the radiation spectra of slowly rotating black holes.

5.2 Flux emission spectra

In the next three subsections, we present the various emission spectra for spin-1/2 fields by using the definitions (3.32)–(3.36) and the exact numerical results for the transmission coefficient discussed above. We start with the particle flux, i.e. the number of fermions emitted by the black hole on the brane per unit time and unit frequency. Figures 4 and 5 depict our results as a function of the dimensionless energy parameter ωr_h and for fixed dimension of spacetime and angular momentum of the black hole, respectively.

The dependence of the particle flux spectrum for fermions follows the same pattern as the one for either scalars [22, 24] or gauge bosons [25]. As either the angular momentum of the black hole or the dimension of spacetime increases, the number of particles emitted by the black hole is greatly enhanced. According to figure 4(a), for low values of n, the black hole clearly tends to emit more low-energy particles than high-energy ones, although as a_* increases the number of the latter becomes significant. For higher values of n, however, as figures 4(b) and 5 reveal, the black hole consistently prefers to emit particles with energies

JHEP03(2007)019

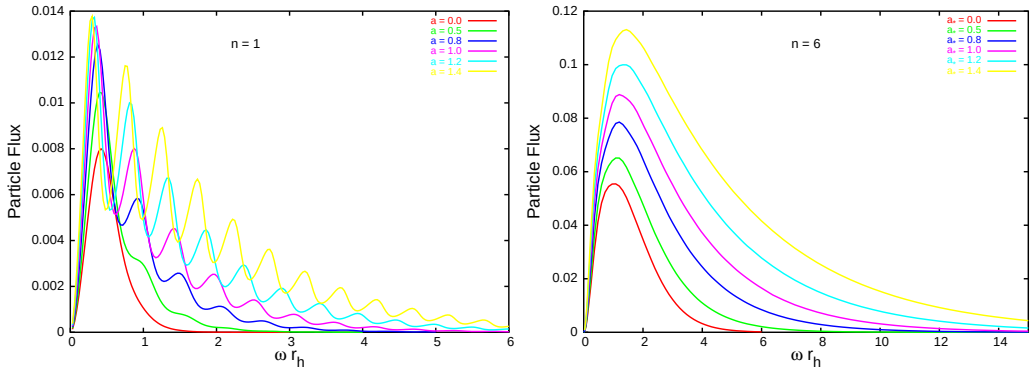

Figure 4: Flux emission spectra for spin-1/2 particles on the brane from a rotating black hole, for **(a)** $n = 1$, and **(b)** $n = 6$, and various values of a_*.

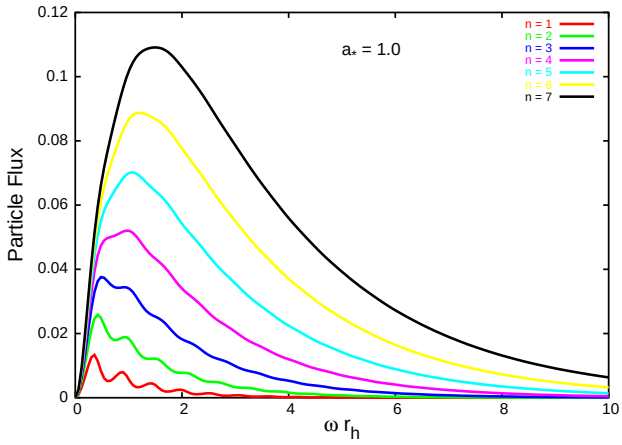

Figure 5: Flux emission spectra for spin-1/2 particles on the brane from a rotating black hole, with $a_* = 1$, for various values of n.

$\omega r_h \geq 1$, with any increase of a_* resulting in the shift of the emission curve towards even larger values of ωr_h.

The angular distribution of the flux spectra of fermionic modes — characteristic in the case of a rotating decaying black hole — was also studied. It was found to borrow features from the corresponding angular distributions of both scalars and gauge bosons. The two indicative cases of $n = 1$ and $n = 6$, for three different values of the angular momentum parameter, i.e. $a_* = (0, 0.6, 1)$, are presented in figures 6 and 7. The depicted spectra correctly reproduce the dependence on a_* and n discussed above, and in addition reveal the existence of two forces that shape the final angular distribution pattern. The centrifugal force, acting on all particles independently of their spin, forces the emitted modes to concentrate on the equatorial plane, i.e. around the value $\theta = \pi/2$ of the azimuthal angle. On the other hand, the non-vanishing spin of the particle leads to a spin-rotation interaction with the angular momentum of the black hole and tends to polarize radiation

JHEP03(2007)019

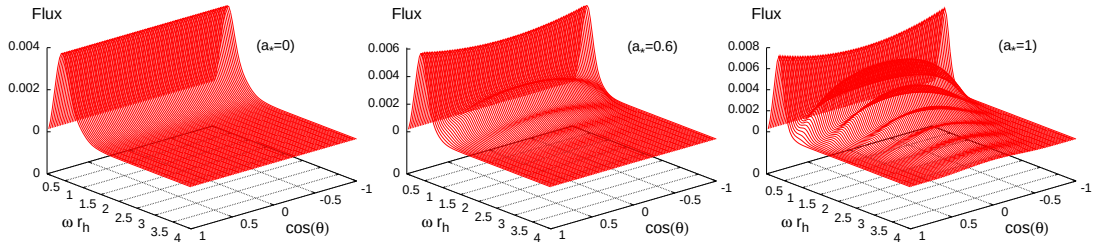

Figure 6: Angular distribution of the flux spectra for emission of fermions on the brane from a rotating black hole, for $n = 1$ and $a_* = (0, 0.6, 1)$.

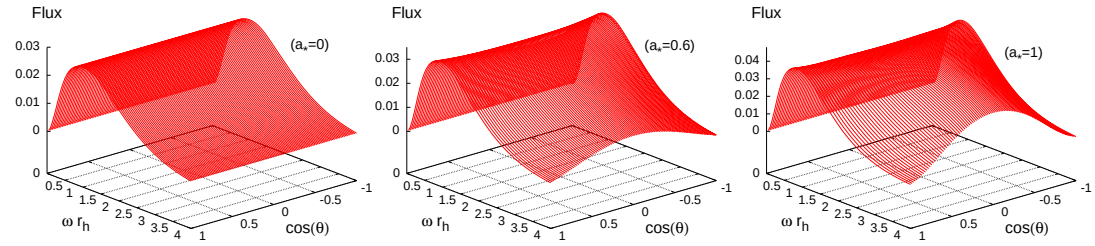

Figure 7: Angular distribution of the flux spectra for emission of fermions on the brane from a rotating black hole, for $n = 6$ and $a_* = (0, 0.6, 1)$.

along the rotation axis ($\theta = 0, \pi$). The latter effect was, as expected, absent in the case of scalar fields [24] but quite prominent in the case of gauge bosons [25]. Here, as expected, it is also present but of a lesser magnitude due to the smaller value of the spin. According to figures 6 and 7, and in agreement with the behaviour found for gauge bosons, the spin-rotation coupling is found to be particularly effective for particles with low energy, but its effect becomes subdominant compared to the one of the centrifugal force as either a_* or n increases — the dying out of the polarization of the radiation along the rotation axis, as the angular momentum of the black hole increases, was also noted in the pure 4-dimensional case [35].

5.3 Power emission spectra

We now turn to the power spectrum, i.e. the energy emitted by the black hole in the form of fermions per unit time and unit frequency. Our results are displayed in figures 8 and 9, again for fixed dimension and angular momentum parameter, respectively. For fixed n, as the angular momentum of the black hole increases, the energy emission curve steadily moves towards larger values of the energy parameter due to the increasingly larger number of high-energy particles emitted, as was observed in the previous subsection.

As a result, significantly larger amounts of energy are radiated away in the high-energy channels than in the low-energy ones compared to the case of a non-rotating black hole. At the same time, each curve becomes taller and wider, thus leading to a total energy emission

JHEP03(2007)019

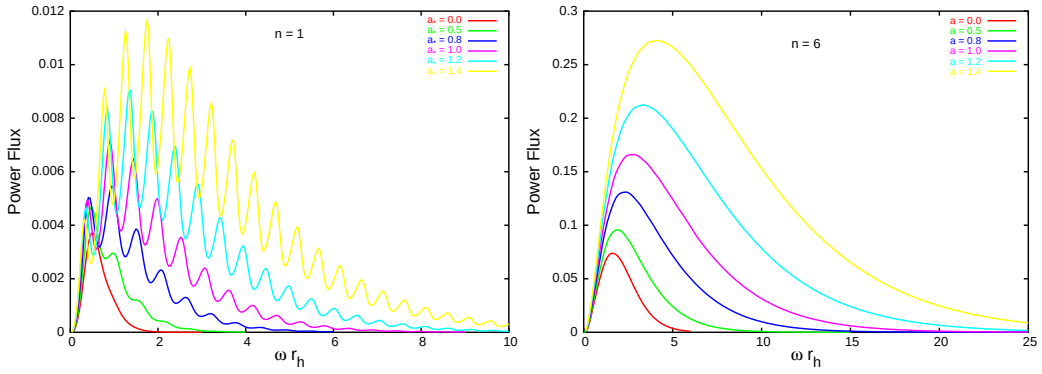

Figure 8: Power emission spectra for spin-1/2 particles on the brane from a rotating black hole, for **(a)** $n = 1$, and **(b)** $n = 6$, and various values of a_*.

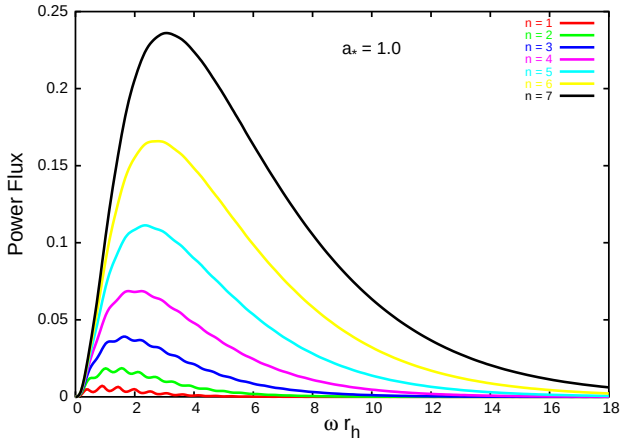

Figure 9: Power emission spectra for spin-1/2 particles on the brane from a rotating black hole, with $a_* = 1$, for various values of n.

rate that is substantially enhanced. According to figure 9, a similar, but significantly more important, enhancement is observed when the dimension of spacetime increases while the angular momentum is kept fixed: a mere comparison of the area outlined by the curves in the two extreme cases of $n = 1$ and $n = 7$ suffices to reveal the enhancement in the emission rate, as the number of the transverse-to-the-brane dimensions increases [2].

The angular distribution of the power spectra for fermion emission on the brane was investigated next, and the results are shown in figures 10 and 11, for the indicative cases again of $n = 1$ and $n = 6$, respectively, and for $a_* = (0, 0.6, 1)$. For $a_* = 0$, the spectrum has no angular dependence as expected, however, as soon as the angular momentum of the

[2] A comparison between our results and the ones produced in [27] for the emission of fermions reveals a discrepancy of 3-5%. This might be due to either the failure of the analytic approximation to the angular eigenvalue used in [27], the potentially different number of partial modes included in the calculation, or simply the different methodology used to determine the transmission coefficient.

JHEP03(2007)019

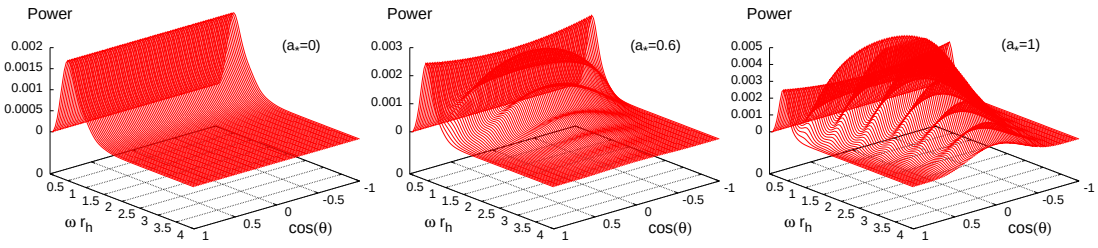

Figure 10: Angular distribution of the power spectra for emission of fermions on the brane from a rotating black hole, for $n = 1$ and $a_* = (0, 0.6, 1)$.

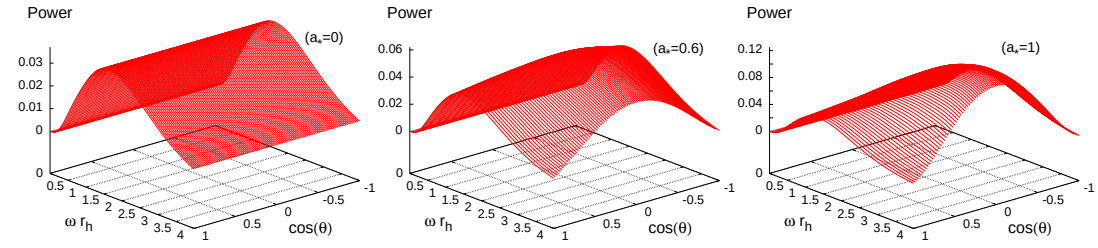

Figure 11: Angular distribution of the power spectra for emission of fermions on the brane from a rotating black hole, for $n = 6$ and $a_* = (0, 0.6, 1)$.

black hole is turned on, the effects of the centrifugal force and the spin-rotation coupling become also apparent here. The latter factor features in the angular distribution pattern only in the low-energy regime and only in the case of low dimension ($n = 1$) — as discussed earlier, as either n or a_* increases, the low-energy part of the spectrum becomes increasingly more suppressed compared to the high-energy one which results also in the disappearance of the polarization of the radiation along the rotation axis. As in the case of the flux spectra, the centrifugal force prevails in the high-energy emission channels, and the bulk of the energy is clearly emitted along the equatorial plane.

5.4 Angular momentum spectra

We now proceed to study the rate of emission of the angular momentum of the black hole, and its dependence on a_* and n. The amount of angular momentum radiated by the black hole per unit time and frequency, is shown in figures 12(a,b) for $n = 1$ and $n = 6$, respectively, and variable a_*, and in figure 13 for fixed a_* and variable n.

As in the case of scalars and gauge bosons, the angular momentum spectrum strongly resembles the power spectrum. As a_* increases, while n remains fixed, the emission curve shifts to the right thus allowing for the loss of the angular momentum of the black hole through the emission of higher energy particles. As either a_* or n increases, the emission curve becomes again wider and taller, thus revealing the fact that rapidly rotating black holes, or black holes living in a spacetime with a large number of transverse dimensions

JHEP03(2007)019

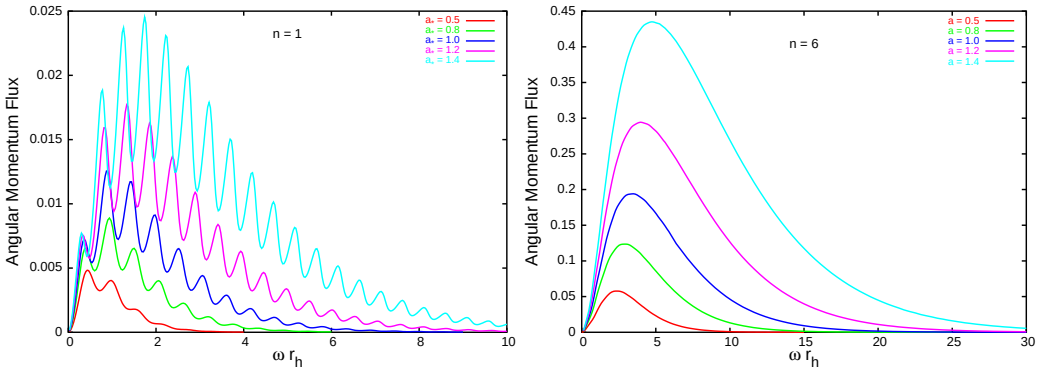

Figure 12: Angular momentum spectra for spin-1/2 particles from a rotating black hole, for **(a)** $n = 1$, and **(b)** $n = 6$, and various values of a_*.

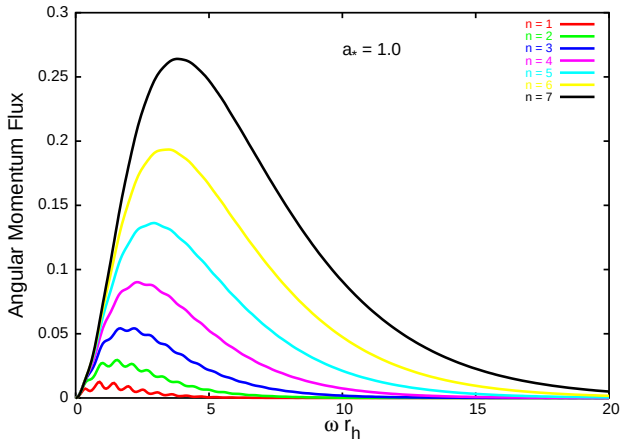

Figure 13: Angular momentum spectra for spin-1/2 particles from a rotating black hole, for $a_* = 1$ and various values of n.

lose their angular momentum much faster.

5.5 Total emissivities

We finally turn to the total emissivities, that describe the emission of either particles, energy or angular momentum per unit time, over the whole frequency band. These total rates follow by integrating the differential emission rates (3.32)–(3.34) over the energy parameter ωr_h. Here, this integration has been performed from zero to a maximum value of the energy parameter, appropriately chosen to cover all the emission for the cases studied. For all three types of spectra, that maximum value was found to be $\omega r_h = 30$. As a result, the computed total emissivities are accurate, and can provide exact enhancement factors for all three types of spectra in terms of a_* and n.

In figures 14(a,b), we present the total emissivities of all three types of emission rates, particle flux, energy and angular momentum, as a function of the number of extra dimensions n and angular momentum parameter a_*, respectively. The first histogram reveals the

JHEP03(2007)019

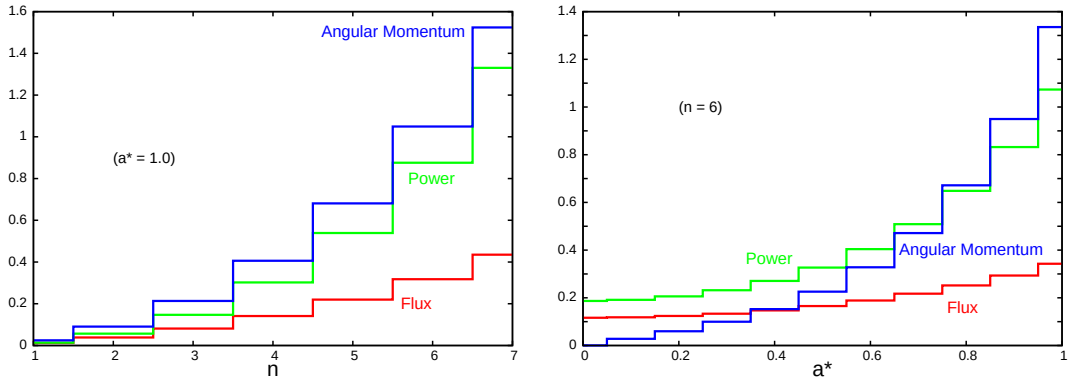

Figure 14: Total emissivities for spin-1/2 particle emission on the brane from a rotating black hole as a function of **(a)** n, for $a_* = 1$, and **(b)** a_*, for $n = 6$.

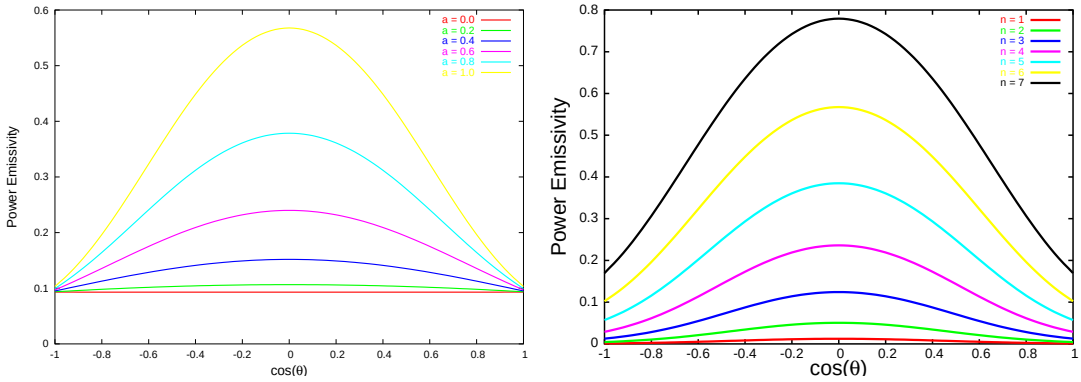

Figure 15: Power emissivity (up to $\omega r_h = 6$) for spin-1/2 emission on the brane from a rotating black hole as a function of $\cos\theta$, **(a)** for $n = 6$ and variable a_*, and **(b)** for $a_* = 1$ and variable n.

enhancement of all three rates, as n increases, while a_* remains fixed ($a_* = 1$). According to our numerical data, as n goes from 1 to 7, the total number of fermions emitted by the black hole per unit time increases by a factor of 35.9, the total energy by a factor of 98.7, and the total angular momentum by a factor of 61.5. The second histogram, figure 14(b), gives the total emissivities when the dimension of spacetime is kept fixed ($n = 6$) and a_* varies. As a_* increases from zero to unity, a significant enhancement takes place again, although of a smaller magnitude: the number of particles emitted per unit time is tripled, while the energy emissivity is enhanced by a factor of 5.7.

Let us finally discuss the angular distribution of energy emitted by the black hole, in the form of fermions, as given by eq. (3.36), but integrated again over the frequency parameter. The derived power emissivity is then a function only of the azimuthal angle θ, and for fixed n and a_*, is depicted in figures 15(a,b), respectively. Similarly to the non-integrated one studied in a previous section, the power emissivity is symmetric with respect to the equatorial plane ($\cos\theta = 0$). The effect of the centrifugal force on the angular distribution of the radiation is also obvious here with the bulk of emitted energy being concentrated on the equatorial plane, for all values of the angular momentum parameter and dimension

JHEP03(2007)019

of spacetime. However, the expected polarisation along the rotation axis caused by the spin-rotation coupling, that gave rise to a twin-peak pattern in a similar plot for gauge bosons [25], is not visible here. This is due to the fact that the low-energy regime, where the spin-rotation coupling is effective, is significantly suppressed when the total emissivities are computed; in addition, the magnitude of this effect for fermions was much smaller in the first place, compared to the ones for gauge bosons, due to the smaller value of their spin. The shape of the fermion power emissivity curves appearing in figures 15 are found to agree with the ones derived in the case of a 4-dimensional, rotating black hole [35].

6. Conclusions

In this work, we have completed the study of the Hawking radiation on the brane from a higher-dimensional rotating black hole by investigating the emission of fermionic modes. A comprehensive analysis was performed that led to the particle, power and angular momentum emission rates, and shed light on their dependence on fundamental parameters of the theory such as the spacetime dimension and angular momentum of the black hole. In addition, the angular distribution of the emitted modes, in terms of number of particles and energy, was thoroughly studied. Our results are valid for arbitrary values of the energy of the emitted particles[3] and angular momentum of the black hole, and complement previous results on the emission of brane-localised scalars [23, 24] and gauge bosons [25].

As in the case of our previous analyses for spin-0 and spin-1 particles, the equation of motion for fermions propagating in the projected-on-the-brane gravitational background needed to be determined first, a task that was performed by employing the Newman-Penrose formalism. The derivation of exact results for the various emission rates demanded the numerical integration of both the angular and radial part of the equation of motion in exactly that order. The former calculation offered exact results for both the angular eigenfunctions, the spin-weighted spheroidal harmonics, and the angular eigenvalues, that also appear in the radial equation. The latter calculation led to exact results for the radial part of the wavefunction of the fermionic field, and eventually for the transmission coefficient.

Our numerical results for the transmission probability as well as for the particle, energy and angular momentum fluxes were presented in section 5. The differential emission rates per unit time and frequency, integrated over the azimuthal angle θ, were addressed first, and spectra for different values of the dimension of spacetime and the angular momentum of the black hole were constructed as a function of the energy of the emitted particle. As in the case of scalars and gauge bosons, it was revealed that any increase in either n or a_* significantly enhances all emission rates of the black hole. The enhancement is present in all frequency regimes, and significantly boosts the emission of higher energy particles

[3]Using the results in [48], we have investigated at what value of ωr_h is the contribution to the spectrum from ultra-short distances (where a full theory of quantum gravity would be required) of the same order as the total spectrum itself. For the main cases plotted in this paper, such value of ωr_h is at the tail-end of the curve for each dominant mode, so that the main contribution to the spectrum is indeed from the semiclassical regime.

JHEP03(2007)019

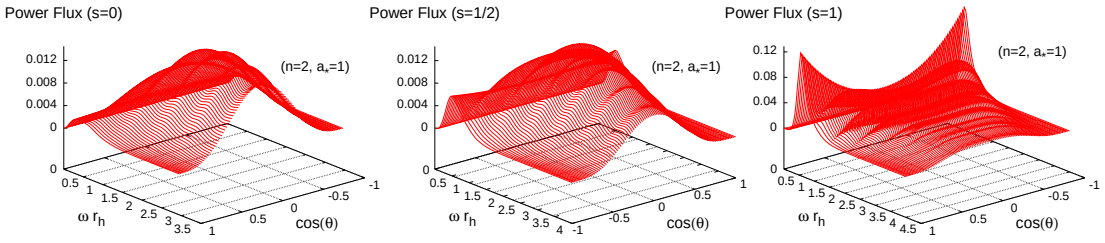

Figure 16: Angular distribution of the power spectra for **(a)** scalars, **(b)** fermions, and **(c)** gauge bosons on the brane from a 6-dimensional black hole with $a_* = 1$.

compared to the case of a non-rotating black hole. Total emissivities, i.e. emission rates integrated over all frequency regimes, were also presented at the end of section 5; these total emission rates confirmed the enhancement of all spectra, in terms of n and a_*, and led to the derivation of the corresponding enhancement factors: as n increases, the various emissivities are enhanced by a factor that varies from 35 to almost 100, while, as a_* grows, this factor is of the order of 3 or 6.

Throughout the study of the emission of various spin-s particles on the brane by a higher-dimensional rotating black hole, a significant amount of energy was invested in the calculation of the exact spin-weighted spheroidal harmonics, that would allow us to determine the exact angular distribution of the emitted particles and energy. Contrary to the case of a spherically-symmetric black hole, the various emission rates for a rotating black hole bear a signature of a characteristic direction in space which is the axis of rotation. It was found that the majority of particles emitted by the black hole are restricted to do so along the equatorial plane due to the strong centrifugal force - this conclusion was reinforced after the total energy emissivities as a function of the azimuthal angle were also computed. Nevertheless, the spin of the particle can significantly affect the angular distribution pattern at the low-energy regime due to the spin-rotation coupling with the angular momentum of the black hole. For comparison, in figures 16(a,b,c) we present the angular distribution of the energy emission spectrum for a 6-dimensional ($n = 2$) rotating black hole emitting radiation on the brane, in the form of scalars [24], fermions and gauge bosons [25], respectively. From these, it becomes obvious that the angular variation in the pattern of the emitted radiation can be a distinctive signature of emission from a rotating black hole, but also of the spin and energy of the particles emitted.

The array of graphs displayed in figure 16 can shed light also on the question of the relative emissivities of different types of particles on the brane from a rotating black hole. In the absence of angular momentum, it was shown [15] that the preference of the black hole for the emission of scalar fields in four dimensions is replaced by the one for gauge bosons when a number of additional spacelike dimensions is introduced. In [25], we were able to show that a higher-dimensional rotating black hole also prefers to emit gauge bosons over scalars on the brane. With the results for fermions being now available, the complete picture has emerged. By merely comparing the vertical axes of the graphs in figure 16,

JHEP03(2007)019

one may see that a higher-dimensional rotating black hole emits approximately the same amount of energy on the brane in the form of scalars and fermions — a more careful comparison of the emission rates integrated over the azimuthal angle, presented in figure 8, with the corresponding ones in [24] reveals that the fermions slightly dominate over the scalars. Nevertheless, as figure 16(c) reveals, a significantly larger amount of energy (by, at least, an order of magnitude) is spent by the black hole in the emission of gauge bosons — the above result holds for all values of n.

The results presented in this work, addressing modifications of the properties of black holes submerged into a higher-dimensional brane-world spacetime, have an obvious theoretical interest. The potential detection of the Hawking radiation from a higher-dimensional black hole formed during a high-energy particle collision in a ground-based accelerator, in the near or far future, increases their significance as the corresponding spectra offer vital information about fundamental parameters of the system under study, such as the dimension of spacetime and angular velocity of the black hole, as well as for the creation of the black hole itself. This information is obtained by looking only at the emission channel along our brane where ordinary Standard Model particles, as well as the potential observers, are restricted to live. With the investigation of the spin-down and Schwarzschild phases of the life of the black hole now completed, what remains to be done is a realistic study of the dynamical evolution of the produced black hole where more advanced aspects, such as the variation of the temperature of the black hole as the decay progresses or the properties and interactions of the Standard Model particles, are properly taken into account. This goal will be achieved by entering our results for the emission of individual scalar, fermionic and gauge bosonic degrees of freedom from a constant-mass black hole into the CHARYBDIS black hole event generator [49]. We hope to report results from this analysis soon.

Acknowledgments

The work of P.K. is funded by the UK PPARC Research Grant PPA/A/S/2002/00350. The work of E.W. is supported by UK PPARC, grant reference number PPA/G/S/2003/00082. M.C. wishes to thank Paul Watts for helpful discussions on the spinor formalism and Jose Navarro-Salas and Ivan Agulló for their insight into transplanckian effects on Hawking radiation spectra.

References

[1] N. Arkani-Hamed, S. Dimopoulos and G.R. Dvali, *The hierarchy problem and new dimensions at a millimeter*, *Phys. Lett.* **B 429** (1998) 263 [hep-ph/9803315]; *Phenomenology, astrophysics and cosmology of theories with sub-millimeter dimensions and TeV scale quantum gravity*, *Phys. Rev.* **D 59** (1999) 086004 [hep-ph/9807344]; I. Antoniadis, N. Arkani-Hamed, S. Dimopoulos and G.R. Dvali, *New dimensions at a millimeter to a Fermi and superstrings at a TeV*, *Phys. Lett.* **B 436** (1998) 257 [hep-ph/9804398].

[2] L. Randall and R. Sundrum, *A large mass hierarchy from a small extra dimension*, *Phys. Rev. Lett.* **83** (1999) 3370 [hep-ph/9905221]; *An alternative to compactification*, *Phys. Rev. Lett.* **83** (1999) 4690 [hep-ph/9906064].

[3] K. Akama, *An early proposal of 'brane world'*, *Lect. Notes Phys.* **176** (1982) 267 [hep-th/0001113];
V.A. Rubakov and M.E. Shaposhnikov, *Extra space-time dimensions: towards a solution to the cosmological constant problem*, *Phys. Lett.* **B 125** (1983) 139; *Do we live inside a domain wall?*, *Phys. Lett.* **B 125** (1983) 136;
M. Visser, *An exotic class of Kaluza-Klein models*, *Phys. Lett.* **B 159** (1985) 22 [hep-th/9910093];
G.W. Gibbons and D.L. Wiltshire, *Space-time as a membrane in higher dimensions*, *Nucl. Phys.* **B 287** (1987) 717;
I. Antoniadis, *A possible new dimension at a few TeV*, *Phys. Lett.* **B 246** (1990) 377;
I. Antoniadis, K. Benakli and M. Quiros, *Production of Kaluza-Klein states at future colliders*, *Phys. Lett.* **B 331** (1994) 313 [hep-ph/9403290];
J.D. Lykken, *Weak scale superstrings*, *Phys. Rev.* **D 54** (1996) 3693 [hep-th/9603133].

[4] T. Banks and W. Fischler, *A model for high-energy scattering in quantum gravity*, hep-th/9906038;
D.M. Eardley and S.B. Giddings, *Classical black hole production in high-energy collisions*, *Phys. Rev.* **D 66** (2002) 044011 [gr-qc/0201034];
H. Yoshino and Y. Nambu, *High-energy head-on collisions of particles and hoop conjecture*, *Phys. Rev.* **D 66** (2002) 065004 [gr-qc/0204060]; *Black hole formation in the grazing collision of high-energy particles*, *Phys. Rev.* **D 67** (2003) 024009 [gr-qc/0209003];
E. Kohlprath and G. Veneziano, *Black holes from high-energy beam-beam collisions*, *JHEP* **06** (2002) 057 [gr-qc/0203093];
V. Cardoso, O.J.C. Dias and J.P.S. Lemos, *Gravitational radiation in D-dimensional spacetimes*, *Phys. Rev.* **D 67** (2003) 064026 [hep-th/0212168];
E. Berti, M. Cavaglia and L. Gualtieri, *Gravitational energy loss in high energy particle collisions: ultrarelativistic plunge into a multidimensional black hole*, *Phys. Rev.* **D 69** (2004) 124011 [hep-th/0309203];
V.S. Rychkov, *Black hole production in particle collisions and higher curvature gravity*, *Phys. Rev.* **D 70** (2004) 044003 [hep-ph/0401116];
S.B. Giddings and V.S. Rychkov, *Black holes from colliding wavepackets*, *Phys. Rev.* **D 70** (2004) 104026 [hep-th/0409131];
O.I. Vasilenko, *Trap surface formation in high-energy black holes collision*, hep-th/0305067;
H. Yoshino and V.S. Rychkov, *Improved analysis of black hole formation in high-energy particle collisions*, *Phys. Rev.* **D 71** (2005) 104028 [hep-th/0503171];
D.C. Dai, G.D. Starkman and D. Stojkovic, *Production of black holes and their angular momentum distribution in models with split fermions*, *Phys. Rev.* **D 73** (2006) 104037 [hep-ph/0605085];
H. Yoshino and R.B. Mann, *Black hole formation in the head-on collision of ultrarelativistic charges*, *Phys. Rev.* **D 74** (2006) 044003 [gr-qc/0605131].

[5] S.B. Giddings and S. Thomas, *High energy colliders as black hole factories: the end of short distance physics*, *Phys. Rev.* **D 65** (2002) 056010 [hep-ph/0106219];
S. Dimopoulos and G. Landsberg, *Black holes at the LHC*, *Phys. Rev. Lett.* **87** (2001) 161602 [hep-ph/0106295];
S. Dimopoulos and R. Emparan, *String balls at the LHC and beyond*, *Phys. Lett.* **B 526** (2002) 393 [hep-ph/0108060];
S. Hossenfelder, S. Hofmann, M. Bleicher and H. Stocker, *Quasi-stable black holes at LHC*, *Phys. Rev.* **D 66** (2002) 101502 [hep-ph/0109085];

JHEP03(2007)019

K. Cheung, *Black hole production and large extra dimensions*, *Phys. Rev. Lett.* **88** (2002) 221602 [hep-ph/0110163];
R. Casadio and B. Harms, *Can black holes and naked singularities be detected in accelerators?*, *Int. J. Mod. Phys.* **A 17** (2002) 4635 [hep-ph/0110255];
S.C. Park and H.S. Song, *Production of spinning black holes at colliders*, *J. Korean Phys. Soc.* **43** (2003) 30 [hep-ph/0111069];
G. Landsberg, *Discovering new physics in the decays of black holes*, *Phys. Rev. Lett.* **88** (2002) 181801 [hep-ph/0112061];
G.F. Giudice, R. Rattazzi and J.D. Wells, *Transplanckian collisions at the LHC and beyond*, *Nucl. Phys.* **B 630** (2002) 293 [hep-ph/0112161];
E.J. Ahn, M. Cavaglia and A.V. Olinto, *Brane factories*, *Phys. Lett.* **B 551** (2003) 1 [hep-th/0201042];
T.G. Rizzo, *Black hole production at the LHC: effects of Voloshin suppression*, *JHEP* **02** (2002) 011 [hep-ph/0201228]; *Warped phenomenology of higher-derivative gravity*, *JHEP* **01** (2005) 025 [hep-ph/0412087];
A.V. Kotwal and C. Hays, *Production and decay of spinning black holes at colliders and tests of black hole dynamics*, *Phys. Rev.* **D 66** (2002) 116005 [hep-ph/0206055];
A. Chamblin and G.C. Nayak, *Black hole production at LHC: string balls and black holes from pp and lead-lead collisions*, *Phys. Rev.* **D 66** (2002) 091901 [hep-ph/0206060];
T. Han, G.D. Kribs and B. McElrath, *Black hole evaporation with separated fermions*, *Phys. Rev. Lett.* **90** (2003) 031601 [hep-ph/0207003];
I. Mocioiu, Y. Nara and I. Sarcevic, *Hadrons as signature of black hole production at the LHC*, *Phys. Lett.* **B 557** (2003) 87 [hep-ph/0310073];
M. Cavaglia, S. Das and R. Maartens, *Will we observe black holes at LHC?*, *Class. and Quant. Grav.* **20** (2003) L205 [hep-ph/0305223];
D. Stojkovic, *Distinguishing between the small ADD and RS black holes in accelerators*, *Phys. Rev. Lett.* **94** (2005) 011603 [hep-ph/0409124];
S. Hossenfelder, *The minimal length and large extra dimensions*, *Mod. Phys. Lett.* **A 19** (2004) 2727 [hep-ph/0410122];
C.M. Harris, M.J. Palmer, M.A. Parker, P. Richardson, A. Sabetfakhri and B.R. Webber, *Exploring higher dimensional black holes at the Large Hadron Collider*, *JHEP* **05** (2005) 053 [hep-ph/0411022];
G.L. Alberghi, R. Casadio, D. Galli, D. Gregori, A. Tronconi and V. Vagnoni, *Probing quantum gravity effects in black holes at LHC*, hep-ph/0601243;
G.C. Nayak and J. Smith, *Higgs boson production from black holes at the LHC*, *Phys. Rev.* **D 74** (2006) 014007 [hep-ph/0602129];
H. Stocker, *Stable TeV - black hole remnants at the LHC: discovery through di-jet suppression, mono-jet emission and a supersonic boom in the quark-gluon plasma*, hep-ph/0605062;
L. Lonnblad and M. Sjodahl, *Classical and non-classical ADD-phenomenology with high-E(T) jet observables at collider experiments*, *JHEP* **10** (2006) 088 [hep-ph/0608210].

[6] A. Goyal, A. Gupta and N. Mahajan, *Neutrinos as source of ultra high-energy cosmic rays in extra dimensions*, *Phys. Rev.* **D 63** (2001) 043003 [hep-ph/0005030];
J.L. Feng and A.D. Shapere, *Black hole production by cosmic rays*, *Phys. Rev. Lett.* **88** (2002) 021303 [hep-ph/0109106];
L. Anchordoqui and H. Goldberg, *Experimental signature for black hole production in neutrino air showers*, *Phys. Rev.* **D 65** (2002) 047502 [hep-ph/0109242];
R. Emparan, M. Masip and R. Rattazzi, *Cosmic rays as probes of large extra dimensions and*

JHEP03(2007)019

TeV gravity, *Phys. Rev.* **D 65** (2002) 064023 [hep-ph/0109287];
L.A. Anchordoqui, J.L. Feng, H. Goldberg and A.D. Shapere, *Black holes from cosmic rays: probes of extra dimensions and new limits on TeV-scale gravity*, *Phys. Rev.* **D 65** (2002) 124027 [hep-ph/0112247]; *Updated limits on TeV scale gravity from absence of neutrino cosmic ray showers mediated by black holes*, *Phys. Rev.* **D 68** (2003) 104025 [hep-ph/0307228];
Y. Uehara, *Production and detection of black holes at neutrino array*, *Prog. Theor. Phys.* **107** (2002) 621 [hep-ph/0110382];
J. Alvarez-Muñiz, J.L. Feng, F. Halzen, T. Han and D. Hooper, *Detecting microscopic black holes with neutrino telescopes*, *Phys. Rev.* **D 65** (2002) 124015 [hep-ph/0202081];
A. Ringwald and H. Tu, *Collider versus cosmic ray sensitivity to black hole production*, *Phys. Lett.* **B 525** (2002) 135 [hep-ph/0111042];
M. Kowalski, A. Ringwald and H. Tu, *Black holes at neutrino telescopes*, *Phys. Lett.* **B 529** (2002) 1 [hep-ph/0201139];
E.J. Ahn, M. Ave, M. Cavaglia and A.V. Olinto, *TeV black hole fragmentation and detectability in extensive air-showers*, *Phys. Rev.* **D 68** (2003) 043004 [hep-ph/0306008];
A. Mironov, A. Morozov and T.N. Tomaras, *Can centauros or chirons be the first observations of evaporating mini black holes?*, hep-ph/0311318;
E.J. Ahn, M. Cavaglia and A.V. Olinto, *Uncertainties in limits on TeV-gravity from neutrino induced air showers*, *Astropart. Phys.* **22** (2005) 377 [hep-ph/0312249];
T. Han and D. Hooper, *The particle physics reach of high-energy neutrino astronomy*, *New J. Phys.* **6** (2004) 150 [hep-ph/0408348];
A. Cafarella, C. Coriano and T.N. Tomaras, *Cosmic ray signals from mini black holes in models with extra dimensions: an analytical / Monte Carlo study*, *JHEP* **06** (2005) 065 [hep-ph/0410358];
D. Stojkovic and G.D. Starkman, *Why black hole production in scattering of cosmic ray neutrinos is generically suppressed*, *Phys. Rev. Lett.* **96** (2006) 041303 [hep-ph/0505112];
A. Barrau, C. Feron and J. Grain, *Astrophysical production of microscopic black holes in a low Planck-scale world*, *Astrophys. J.* **630** (2005) 1015 [astro-ph/0505436];
L. Anchordoqui, T. Han, D. Hooper and S. Sarkar, *Exotic neutrino interactions at the Pierre Auger observatory*, *Astropart. Phys.* **25** (2006) 14 [hep-ph/0508312];
E.J. Ahn and M. Cavaglia, *Simulations of black hole air showers in cosmic ray detectors*, *Phys. Rev.* **D 73** (2006) 042002 [hep-ph/0511159].

[7] P. Kanti, *Black holes in theories with large extra dimensions: a review*, *Int. J. Mod. Phys.* **A 19** (2004) 4899 [hep-ph/0402168].

[8] M. Cavaglia, *Black hole and brane production in TeV gravity: a review*, *Int. J. Mod. Phys.* **A 18** (2003) 1843 [hep-ph/0210296];
G. Landsberg, *Black holes at future colliders and in cosmic rays*, *Eur. Phys. J.* **C 33** (2004) S927 [hep-ex/0310034];
K. Cheung, *Collider phenomenology for a few models of extra dimensions*, hep-ph/0409028;
S. Hossenfelder, *What black holes can teach us*, hep-ph/0412265;
A.S. Majumdar and N. Mukherjee, *Braneworld black holes in cosmology and astrophysics*, *Int. J. Mod. Phys.* **D 14** (2005) 1095 [astro-ph/0503473];
A. Casanova and E. Spallucci, *TeV mini black hole decay at future colliders*, *Class. and Quant. Grav.* **23** (2006) R45 [hep-ph/0512063].

[9] C.M. Harris, *Physics beyond the standard model: exotic leptons and black holes at future colliders*, hep-ph/0502005.

JHEP03(2007)019

[10] P.C. Argyres, S. Dimopoulos and J. March-Russell, *Black holes and sub-millimeter dimensions*, *Phys. Lett.* **B 441** (1998) 96 [hep-th/9808138].

[11] S.W. Hawking, *Particle creation by black holes*, *Commun. Math. Phys.* **43** (1975) 199.

[12] P. Kanti and J. March-Russell, *Calculable corrections to brane black hole decay. I: the scalar case*, *Phys. Rev.* **D 66** (2002) 024023 [hep-ph/0203223].

[13] V.P. Frolov and D. Stojkovic, *Black hole radiation in the brane world and recoil effect*, *Phys. Rev.* **D 66** (2002) 084002 [hep-th/0206046].

[14] P. Kanti and J. March-Russell, *Calculable corrections to brane black hole decay. II: Greybody factors for spin* 1/2 *and* 1, *Phys. Rev.* **D 67** (2003) 104019 [hep-ph/0212199].

[15] C.M. Harris and P. Kanti, *Hawking radiation from a* $(4+n)$*-dimensional black hole: exact results for the Schwarzschild phase*, *JHEP* **10** (2003) 014 [hep-ph/0309054].

[16] P. Kanti, J. Grain and A. Barrau, *Bulk and brane decay of a (4+n)-dimensional Schwarzschild-de-Sitter black hole: scalar radiation*, *Phys. Rev.* **D 71** (2005) 104002 [hep-th/0501148].

[17] A. Barrau, J. Grain and S.O. Alexeyev, *Gauss-Bonnet black holes at the LHC: beyond the dimensionality of space*, *Phys. Lett.* **B 584** (2004) 114;
J. Grain, A. Barrau and P. Kanti, *Exact results for evaporating black holes in curvature-squared Lovelock gravity: Gauss-Bonnet greybody factors*, *Phys. Rev.* **D 72** (2005) 104016 [hep-th/0509128];
T.G. Rizzo, *TeV-scale black hole lifetimes in extra-dimensional Lovelock gravity*, *Class. and Quant. Grav.* **23** (2006) 4263 [hep-ph/0601029]; *Higher curvature gravity in TeV-scale extra dimensions*, hep-ph/0603242.

[18] E. Jung and D.K. Park, *Absorption and emission spectra of an higher-dimensional Reissner-Nordstroem black hole*, *Nucl. Phys.* **B 717** (2005) 272 [hep-th/0502002];
E. Jung, S. Kim and D.K. Park, *Ratio of absorption cross section for Dirac fermion to that for scalar in the higher-dimensional black hole background*, *Phys. Lett.* **B 614** (2005) 78 [hep-th/0503027];
S. Q. Wu and Q.Q. Jiang, *Hawking radiation of charged particles as tunneling from higher dimensional Reissner-Nordstroem-de Sitter black holes*, hep-th/0603082.

[19] E.l. Jung, S.H. Kim and D.K. Park, *Absorption cross section for s-wave massive scalar*, *Phys. Lett.* **B 586** (2004) 390 [hep-th/0311036]; *Low-energy absorption cross section for massive scalar and Dirac fermion by* $(4+n)$*-dimensional Schwarzschild black hole*, *JHEP* **09** (2004) 005 [hep-th/0406117]; *Proof of universality for the absorption of massive scalar by the higher-dimensional Reissner-Nordstroem black holes*, *Phys. Lett.* **B 602** (2004) 105 [hep-th/0409145];
M. Doran and J. Jaeckel, *Testing dark energy and light particles via black hole evaporation at colliders*, astro-ph/0501437.

[20] A.S. Cornell, W. Naylor and M. Sasaki, *Graviton emission from a higher-dimensional black hole*, *JHEP* **02** (2006) 012 [hep-th/0510009];
D.K. Park, *Hawking radiation of the brane-localized graviton from a* $(4+n)$*-dimensional black hole*, *Class. and Quant. Grav.* **23** (2006) 4101 [hep-th/0512021];
Emissivities for the various graviton modes in the background of the higher-dimensional black hole, *Phys. Lett.* **B 638** (2006) 246 [hep-th/0603224];

JHEP03(2007)019

V. Cardoso, M. Cavaglia and L. Gualtieri, *Black hole particle emission in higher-dimensional spacetimes*, *Phys. Rev. Lett.* **96** (2006) 071301 [Erratum: *ibid.* **96** (2006) 219902] [hep-th/0512002]; *Hawking emission of gravitons in higher dimensions: non-rotating black holes JHEP* **02** (2006) 021 [hep-th/0512116];
S. Creek, O. Efthimiou, P. Kanti and K. Tamvakis, *Graviton emission in the bulk from a higher-dimensional Schwarzschild black hole*, *Phys. Lett.* **B 635** (2006) 39 [hep-th/0601126].

[21] V.P. Frolov and D. Stojkovic, *Quantum radiation from a* 5*-dimensional rotating black hole*, *Phys. Rev.* **D 67** (2003) 084004 [gr-qc/0211055].

[22] D. Ida, K.y. Oda and S.C. Park, *Rotating black holes at future colliders: greybody factors for brane fields*, *Phys. Rev.* **D 67** (2003) 064025 [Erratum: *ibid.* **69** (2004) 049901] [hep-th/0212108].

[23] C.M. Harris and P. Kanti, *Hawking radiation from a* $(4 + n)$*-dimensional rotating black hole*, *Phys. Lett.* **B 633** (2006) 106 [hep-th/0503010].

[24] G. Duffy, C. Harris, P. Kanti and E. Winstanley, *Brane decay of a* $(4 + n)$*-dimensional rotating black hole: spin-0 particles*, *JHEP* **09** (2005) 049 [hep-th/0507274].

[25] M. Casals, P. Kanti and E. Winstanley, *Brane decay of a* $(4 + n)$*-dimensional rotating black hole. II: spin-*1 *particles*, *JHEP* **02** (2006) 051 [hep-th/0511163].

[26] D. Ida, K.y. Oda and S.C. Park, *Rotating black holes at future colliders. II: anisotropic scalar field emission*, *Phys. Rev.* **D 71** (2005) 124039 [hep-th/0503052].

[27] D. Ida, K.y. Oda and S.C. Park, *Rotating black holes at future colliders. III: determination of black hole evolution*, *Phys. Rev.* **D 73** (2006) 124022 [hep-th/0602188].

[28] D. Ida, K.y. Oda and S.C. Park, *Anisotropic scalar field emission from TeV scale black hole*, hep-ph/0501210;
E. Jung, S. Kim and D.K. Park, *Condition for superradiance in higher-dimensional rotating black holes*, *Phys. Lett.* **B 615** (2005) 273 [hep-th/0503163]; *Condition for the superradiance modes in higher-dimensional rotating black holes with multiple angular momentum parameters*, *Phys. Lett.* **B 619** (2005) 347 [hep-th/0504139].

[29] H. Nomura, S. Yoshida, M. Tanabe and K.i. Maeda, *The fate of a five-dimensional rotating black hole via Hawking radiation*, *Prog. Theor. Phys.* **114** (2005) 707 [hep-th/0502179];
E. Jung and D.K. Park, *Bulk versus brane in the absorption and emission:* 5*D rotating black hole case*, *Nucl. Phys.* **B 731** (2005) 171 [hep-th/0506204].

[30] R.C. Myers and M.J. Perry, *Black holes in higher dimensional space-times*, *Ann. Phys. (NY)* **172** (1986) 304.

[31] S.S. Seahra, *Naked shell singularities on the brane*, *Phys. Rev.* **D 71** (2005) 084020 [gr-qc/0501018];
C. Galfard, C. Germani and A. Ishibashi, *Asymptotically AdS brane black holes*, *Phys. Rev.* **D 73** (2006) 064014 [hep-th/0512001];
S. Creek, R. Gregory, P. Kanti and B. Mistry, *Braneworld stars and black holes*, *Class. and Quant. Grav.* **23** (2006) 6633 [hep-th/0606006].

[32] N. Kaloper and D. Kiley, *Exact black holes and gravitational shockwaves on codimension-*2 *branes*, *JHEP* **03** (2006) 077 [hep-th/0601110].

JHEP03(2007)019

[33] S.A. Teukolsky, *Rotating black holes - separable wave equations for gravitational and electromagnetic perturbations*, *Phys. Rev. Lett.* **29** (1972) 1114; *Perturbations of a rotating black hole. 1. Fundamental equations for gravitational electromagnetic, and neutrino field perturbations*, *Astrophys. J.* **185** (1973) 635.

[34] S. Chandrasekhar, *The mathematical theory of black holes*, Oxford University Press, New York (1983).

[35] D.A. Leahy and W.G. Unruh, *Angular dependence of neutrino emission from rotating black holes*, *Phys. Rev.* **D 19** (1979) 3509.

[36] W.G. Unruh, *Separability of the neutrino equations in a Kerr background*, *Phys. Rev. Lett.* **31** (1973) 1265; *Second quantization in the Kerr metric*, *Phys. Rev.* **D 10** (1974) 3194; *Absorption cross-section of small black holes*, *Phys. Rev.* **D 14** (1976) 3251.

[37] A. Vilenkin, *Parity nonconservation and rotating black holes*, *Phys. Rev. Lett.* **41** (1978) 1575.

[38] P.A. Bolashenko and V.P. Frolov, *Quantum effects for massless spin particles in a gravitational field of a rotating black hole*, *Trudy Fiz. Inst. Lebedev* **197** (1989) 88.

[39] D.R. Brill and J.A. Wheeler, *Interaction of neutrinos and gravitational fields*, *Rev. Mod. Phys.* **29** (1957) 465.

[40] P.B. Groves, P.R. Anderson and E.D. Carlson, *Method to compute the stress-energy tensor for the massless spin* 1/2 *field in a general static spherically symmetric spacetime*, *Phys. Rev.* **D 66** (2002) 124017 [gr-qc/0207066].

[41] V.P. Frolov and I.G. Novikov, *Black hole physics: basic concepts and new developments*, Kluwer, Netherlands (1998).

[42] W.G. Unruh, *Notes on black hole evaporation*, *Phys. Rev.* **D 14** (1976) 870.

[43] C.Y. Cardall and G.M. Fuller, *Neutrino oscillations in curved spacetime: an heuristic treatment*, *Phys. Rev.* **D 55** (1997) 7960 [hep-ph/9610494].

[44] S.A. Hughes, *Evolution of circular, non-equatorial orbits of Kerr black holes due to gravitational wave emission*, *Phys. Rev.* **D 61** (2000) 084004.

[45] E.W. Leaver, *An analytic representation for the quasi-normal modes of Kerr black holes*, *Proc. R. Soc. London A* **402** (1985) 285.

[46] W.H. Press, S.A. Teukolsky, W.T. Vetterling and B.P. Flannery, *Numerical recipes in Fortran*, Cambridge University Press, Cambridge (2002).

[47] M. Casals and A.C. Ottewill, *High frequency asymptotics for the spin-weighted spheroidal equation*, *Phys. Rev.* **D 71** (2005) 064025 [gr-qc/0409012];
M. Casals, Ph.D. thesis, University College Dublin (2004).

[48] I. Agulló, J. Navarro-Salas and G.J. Olmo, *Short distances, black holes, and TeV gravity*, hep-th/0701162.

[49] C.M. Harris, P. Richardson and B.R. Webber, *CHARYBDIS: a black hole event generator*, *JHEP* **08** (2003) 033 [hep-ph/0307305].

JHEP03(2007)019